Thanh, Cuong-Le; Tran, Loc V.; Vu-Huu, T.; Nguyen-Xuan, H.; Abdel-Wahab, M.

Size-dependent nonlinear analysis and damping responses of FG-CNTRC micro-plates

Published in:
Computer Methods in Applied Mechanics and Engineering

DOI:
10.1016/j.cma.2019.05.002

Published: 15/08/2019

Document Version
Peer-reviewed accepted author manuscript, also known as Final accepted manuscript or Post-print

Accepted Manuscript

Size-dependent nonlinear analysis and damping responses of FG-CNTRC micro-plates

Cuong-Le Thanh, Loc V. Tran, T. Vu-Huu, H. Nguyen-Xuan, M. Abdel-Wahab

PII: S0045-7825(19)30261-0
DOI: https://doi.org/10.1016/j.cma.2019.05.002
Reference: CMA 12436

To appear in: *Comput. Methods Appl. Mech. Engrg.*

Received date : 20 March 2019
Revised date : 2 May 2019
Accepted date : 5 May 2019

Size-dependent nonlinear analysis and damping responses of FG-CNTRC micro-plates

Cuong-Le Thanh[a,b], Loc V. Tran[e], T. Vu-Huu[a] , H. Nguyen-Xuan[f,g], M. Abdel-Wahab[c,d]*

[a]Department of Electrical energy, metals, mechanical constructions and systems, Soete Laboratory, Faculty of Engineering and Architecture, Ghent University, Belgium
[b]Faculty of Civil Engineering and Electricity, Open University, Ho Chi Minh City, Vietnam
[c]Division of Computational Mechanics, Ton Duc Thang University, Ho Chi Minh City, Vietnam
[d]Faculty of Civil Engineering, Ton Duc Thang University, Ho Chi Minh City, Vietnam
[e] Department of Civil Engineering, School of Engineering, Aalto University, Finland
[f]CIRTECH Institute, Ho Chi Minh City University of Technology (HUTECH), Ho Chi Minh City, Vietnam
[g]Department of Architectural Engineering, Sejong University, 98 Gunja-dong, Gwangjin-gu, Seoul 143-747, South Korea

*Corresponding author: magd.abdelwahab@tdt.edu.vn

A B S T R A C T

This paper presents a nonlinear numerical model, which is based on the modified couple stress theory (MCST), and trigonometric shear deformation theory coupled with isogeometric analysis. The present approach captures the small scale effects on the geometrically nonlinear behaviors of functionally graded carbon nanotube reinforced composite (FG-CNTRC) micro-plate with four patterns distribution. The equations of motion are established based on a Garlekin weak form associated with von-Kármán nonlinear strains. The MCST utilizes only one material length scale parameter to predict the size effect in FG-CNTRC micro-plate, for which its material properties are derived from an extended rule of mixture. The solutions of nonlinear static equation are obtained by using the Newton-Raphson technique and the Newmark time iteration procedure in association with Picard method is assigned to get responses of the nonlinear dynamic problems. In addition, the Rayleigh damping is applied to consider the influence of damping characteristic on the oscillation of FG-CNTRC micro-plates. Comparisons are performed to verify the proposed approach. Afterward, the numerical examples are used to show the effects of the distribution of carbon nanotubes (CNT), their volume fraction, the material length scale parameter and the boundary conditions on the nonlinear static and dynamic behaviors of FG-CNTRC micro-plates.

Keywords: Nonlinear static; Nonlinear dynamic; size-dependent; Modified couple stress theory; Functionally graded carbon nanotube.

1. Introduction

During the last decade, many scientists focus on studying the size or small scale effects on micro- and nano-structures, which are widely used in micro-electromechanical systems (MEMS), nano-electromechanical systems (NEMS) biosensors and atomic force microscopes [1-4]. In fact, in contrast to macro-mechanical behaviors, experimental measurements pointed out that the strength and stiffness of micro and nano-scale material were higher than their bulky materials. Through torsional experiments on Cu wires, Fleck et al. [5] showed that the decrease in wire diameter from 170 μm to 12 μm led to a systematic increase in torsion. For computing the plasticity length scale, Stolken et al. [6] presented a flexible micro-bending test method with the range of length scale from 3 μm to 5 μm to the measured moment. Chong et al. [7] performed experimental investigation to determine the influences of strain gradient on plastic deformation through nano-indentation and atomic force microscopy. By experimental measurements, Lam et al. [8] proved that strain gradients played a main role in the elastic deformation of thin beams, and also in determining the small-scale effect of MEMS and NEMS. However, the conventional elasticity theories is not capable of capturing the size effect of the small scale structures when the material size lies below approximately 10 μm [5].

Various non-classical elasticity theories calculate both strain and strain gradients to determine the scale effect using material length scale (MLS) parameter. Toupin [9], Mindlin and Tiersten [10], Koiter [11] proposed the couple stress theories that considered only gradient of rotation vector in the strain energy with two MLS parameters. Furthermore, Fleck and Hutchinson [12] and Lam et al. [8] recommended strain gradient theory that employed three MLS parameters to apprehend the small scale effect. Owing to the difficulty of resolving more than one MLS parameter, Yang et al. [13] established the modified couple stress theory (MCST) based on amending the couple stress theory using the symmetric couple stress tensor in equilibrium relation condition. This theory contains one MLS parameter, and it is simpler and easier to apply than any other strain gradient theory.

Based on non-classical theories, many numerical and analytical models have been established to predict the responses of micro- and sub-micro structures. An early nonlocal plate solution was presented by Lu et al. [14] for the bending and buckling analysis of isotropic nano-plates. The variable transformation technique was applied by Duan and Wang [15] to obtain the exact nonlocal solution that predicted the axisymmetric bending responses of circular micro-/nano-plate subjected general loading. Reddy [16] proposed a nonlocal solution to solve the nonlinear problems of isotropic nano-plates. By using refined plate theory and nonlocal elasticity theory, Nguyen et al. [17] studied the size-dependent effect on bending, free vibration and buckling phenomenon of functionally graded (FG) nano-plates. Thai et al. [18] proposed an MCST Timoshenko beam to predict the static, dynamic and buckling behaviors of FG sandwich micro-beam. Wang et al. [19] derived a nonlinear MCST solution to study the small scale effect on nonlinear free vibration of circular micro-plate under clamped and simply supported boundary condition. Wang et al. [20] also extended the research to investigate the nonlinear bending of circular micro-plate under uniformly distributed transverse load. The MCST was first coupled with third order shear deformation theory (TSDT) by Gao et al. [21] to depict the influence of small size-dependent on static bending and free vibration of micro-plate under simply supported boundary condition. Based on von-Kármán nonlinear strains and MCST, Reddy and Kim [22] achieved a small size-dependent model for nonlinear responses of functionally graded micro-plate. Nguyen et al. [23] also obtained a MCST refined plate quasi-3D isogeometric solution for FG micro-plate. More recently, Thanh et al. [24] established a numerical model for thermal bending and buckling analysis of composite laminated micro-plate based on the new MCST. The nonlocal and strain gradient elasticity theory was also utilized to establish a Navier closed form solution by Karami et al. [25] for resonance vibration of functionally graded polymer composite reinforced with grapheme nanoplatelets. Based nonlocal strain gradient theory, Karami et al [26] developed a size-dependent analytical solution to capture the small-scale effect on wave dispersion in anisotropic doubly-curved nanoshells. Furthermore, Karami and Janghorban [27] presented a three dimensional elasticity theory for small-scale effect analysis of anisotropic solid sphere. They also studied the size effects on dynamic behavior of porous nanotubes using Timoshenko beam theory [28], and obtained a 3D elastic theory for anisotropic spherical nanoparticle [29]. Furthermore, a number size-dependent models have been formed according to modified strain gradient theory coupled with beam and plate theories [30-33].

Thanks to the extraordinary properties of CNTRC material [34-39], research on behaviors of CNTRC micro-/nano-beam and plate subjected thermal and mechanical load has gained increasing attention. In particular, Shahrisri et al. [40] presented an analytical Mindlin's strain gradient TSDT solution to predict the natural frequencies of simply supported nano-plate. By using nonlocal theory and Navier's method, Ghorbanpour Arani et al. [41] obtained a closed form solution to analyze the surface stress effect on buckling nano-composite plate reinforced by CNTs. Mohammadimehr et al. [42] presented a modified strain gradient TSDT model for FG-SWCNTs nano-composite plate. A closed form solution for bending and buckling of simply supported plate were also derived. In addition, Mohammadimehr et al. [43] investigated the buckling and vibration behaviors of double-bonded piezoelectric nano-composite plate on Pasternak foundation. The small size-dependent effect on the behaviors of nano-plate was derived from the MCST. Karami et al. [44] generated a nonlocal SSDT model for FG-CNTRC plate on Winkler–Pasternak elastic foundation. The analytical solutions for static bending, free vibration and buckling were also obtained for FG-CNTRC plates.

In order to fill the gap between CAD and FEA, NURBS based isogeometric analysis was introduced in 2005 [45]. In engineering design, the non-uniform rational B-splines (NURBS) is the most widely utilized. NURBS is used as shape function to approximate both geometric model and analysis model (unknown field). Additionally, NURBS provides a flexible way to make refinement, de-refinement, and degree elevation [46], and makes it easy to obtain C^{p-1}-continuity for p^{th}-order. Therefore, the accuracy of the analysis of complex structures with the geometry domain like spheres, cylinder, circle, etc. is obtained. IGA has been widely implemented in developing the numerical solutions for mechanical problems [47-53]. Moreover, IGA [45] has been assigned to achieve several size-dependent numerical solutions for micro- and nano-plates [54-60].

From the above literature, there are few approaches including the size parameters for analysis of the small size-dependent effects on FG-CNTRC plates at the order of micro and submicron sizes. Furthermore, the damping characteristic of CNTRC structures was not considered due to reinforced CNT [61-63]. The experimental work showed that a 200% increase in damping ability was observed by CNT reinforcement [62], and therefore the CNT reinforced composite structure can significantly dissipate the energy during oscillation. To the best of our awareness, there is no publication that analyzes the small scale effect on nonlinear static and nonlinear dynamic taking into account damping property of FG-CNTRC micro-plates. By using Hamilton's principle, a nonlinear size-dependent Garlekin weak form is established based on a proposed trigonometric shear deformation theory and von-Kármán assumption. Moreover, nonlinear dynamic analysis of FG-CNTRC micro-plate accounts for the effect of structural damping that is calculated with Rayleigh damping. Newton-Raphson technique and the Newmark's integration coupled with Picard method are assigned to explore the nonlinear static and dynamic responses of FG-CNTRC micro-plate, respectively. This study also clearly investigates the influences of MLS parameter, CNT volume fraction, patterns of CNT distribution and boundary conditions on nonlinear deflection of micro-plates.

2. Theoretical formulations

2.1. FG-CNTRC definition

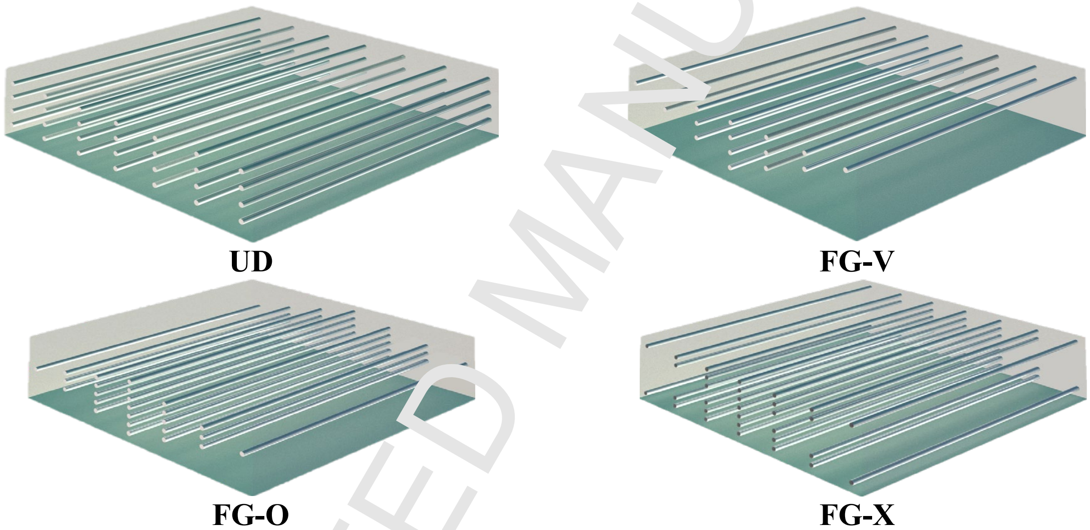

Fig. 1. Configuration of FG-CNTRC micro-plate with four patterns distribution of CNT: UD; FG-V; FG-O; FG-X.

Suppose that a FG-CNTRC micro-plates are procedure from the isotropic matrix reinforced single-wall carbon nanotubes (SWCNTs) that vary across the thickness direction as shown in Fig. 1, the effective material properties of CNTs reinforced composite micro-plates are predicted based on the Mori-Tanaka scheme [64, 65] or the extend rule of mixtures [66, 67]. According to Shen [67], the effective material properties of mixture CNTs and isotropic matrix are calculated as follows:

$$\begin{aligned}
&E_{11} = \eta_1 V_{CNT} E_{11}^{CNT} + V_m E_m \\
&\frac{\eta_2}{E_{22}} = \frac{V_{CNT}}{E_{22}^{CNT}} + \frac{V_m}{E_m} \\
&\frac{\eta_3}{G_{12}} = \frac{V_{CNT}}{G_{12}^{CNT}} + \frac{V_m}{G_m} \\
&\upsilon_{12} = V_{CNT}^{*} \upsilon_{12}^{CNT} + V_m \upsilon_m \\
&\rho = \rho_{CNT} V_{CNT} + \rho_m V_m
\end{aligned} \tag{1}$$

in which, E_{11}^{CNT}, E_{22}^{CNT} and G_{12}^{CNT}, denote the Young's modulus and shear modulus of CNTs, respectively. η_1, η_2 and η_3 denote the CNTs efficiency parameters that are given in Table 1. E_m and G_m are the Young's modulus and shear modulus of isotropic matrix, respectively. υ_{12}^{CNT} and υ_m are the Poisson's ratio of the CNTs and isotropic matrix, respectively. ρ_{CNT} and ρ_m are the density of the CNTs and isotropic matrix. It is noted that the efficiency parameters were derived from the molecular dynamic simulation based on the rule of mixture [68].

Table 1
The CNT efficiency parameters for different volume fraction

V_{CNT}^{*}	η_1	η_2	η_3
0.11	0.149	0.934	0.934
0.14	0.150	0.941	0.941
0.17	0.149	1.381	1.381

Additionally, V_{CNT} and V_m, respectively, are the volume fraction of CNTs and matrix that observe the equation such as:

$$V_{CNT} + V_m = 1 \tag{2}$$

As shown in Fig. 1, the CNTs are uniformly distributed through the plate's thickness and three others patterns of distribution of CNTs are FG-V, FG-O, FG-X are presented. Consequently, the volume faction depend on pattern of CNTs distribution can be calculated as follows:

$$V_{CNT}=\begin{cases} V_{CNT}^{*} & \text{(UD)} \\ \left(1+\dfrac{2z}{h}\right)V_{CNT}^{*} & \text{(FG-V)} \\ 2\left(1-\dfrac{2|z|}{h}\right)V_{CNT}^{*} & \text{(FG-O)} \\ \dfrac{4|z|}{h}V_{CNT}^{*} & \text{(FG-X)} \end{cases} \tag{3}$$

in which,

$$V_{CNT}^{*}=\frac{w_{CNT}}{w_{CNT}+\left(\rho_{CNT}/\rho_m\right)-\left(\rho_{CNT}/\rho_m\right)w_{CNT}} \tag{4}$$

where, the w_{CNT}, ρ_{CNT} and ρ_m are the mass fraction of CNTs, densities of the CNTs and matrix, respectively.

2.2. A size-dependent model for FG-CNTRC micro-plate

Conforming to the generalized shear deformation plate theory as [69-71], the displacement field of any points in the FG-CNTRC plate within a domain $V=\Omega\mathrm{x}\left(-\frac{h}{2},\frac{h}{2}\right)$ can be expressed as:

$$\begin{aligned} u(x,y,z)&=u_0(x,y)-z\frac{\partial w_0(x,y)}{\partial x}+f\left(z\right)\beta_x(x,y) \\ v(x,y,z)&=v_0(x,y)-z\frac{\partial w_0(x,y)}{\partial y}+f\left(z\right)\beta_y(x,y) \qquad ;\left(\frac{-h}{2}\le z\le\frac{h}{2}\right) \\ w(x,y,z)&=w_0(x,y) \end{aligned} \tag{5}$$

in which, $(u_0,\ v_0)$ are the in-plane displacements along the x and y coordinates and w_0 is the transverse displacement along the z coordinate. β_x and β_y denote the rotation components around the y-axis and x-axis of cross-sections in x-z and y-z planes, respectively. A trigonometric function $f\left(z\right)=\frac{h}{\pi}\ln\left(\sin\left(\pi z/h\right)+\sqrt{\left(\sin\left(\pi z/h\right)\right)^2+1}\right)$ is chosen as the shape function that is utilized to define the transverse shear strains and stresses. From Fig. 2, it is clearly seen that the first derivative of shape function has a zero value at the top and bottom surfaces of plate. Hence, the free shear stress condition at $z=\pm h/2$ is also satisfied. Additionally, three others shape functions and their derivative proposed by Reddy [72], Soldatos [73] and Nguyen-Xuan et al. [74] are illustrated in Fig. 2.

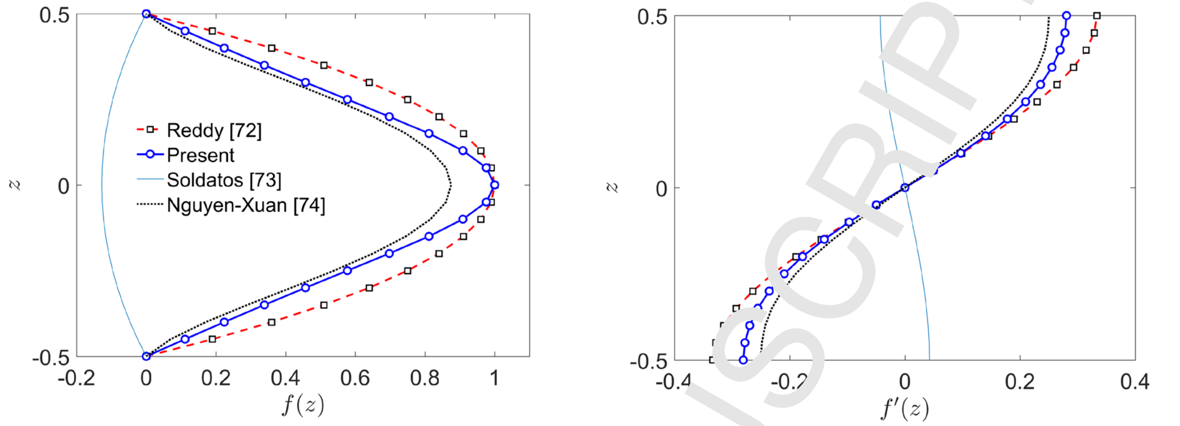

Fig. 2. Shape function $f(z)$ and its first derivative $f'(z)$ across the plate's thickness.

The nonlinear von-Kármán strain-displacement relations with the small strain and moderately large rotation assumption are defined based on the displacement field in Eq. (5) and are presented in a compact form as:

$$\begin{aligned} \boldsymbol{\varepsilon} &= \left\{\varepsilon_x \ \varepsilon_y \ \gamma_{xy}\right\}^T = \boldsymbol{\varepsilon}_0 + z\boldsymbol{\kappa}_1 + f(z)\boldsymbol{\kappa}_2 \\ \boldsymbol{\gamma} &= \left\{\gamma_{xz} \ \gamma_{yz}\right\}^T = f'(z)\boldsymbol{\varepsilon}_s \end{aligned} \tag{6}$$

in which,

$$\begin{aligned} &\boldsymbol{\varepsilon}_0 = \boldsymbol{\varepsilon}_0^L + \boldsymbol{\varepsilon}_0^{NL} = \begin{Bmatrix} u_{0,x} \\ v_{0,y} \\ u_{0,y} + v_{0,x} \end{Bmatrix} + \frac{1}{2}\begin{Bmatrix} w_{0,x}^2 \\ w_{0,y}^2 \\ 2w_{0,x}w_{0,y} \end{Bmatrix} \\ &\boldsymbol{\kappa}_1 = -\begin{Bmatrix} w_{0,xx} \\ w_{0,yy} \\ 2w_{0,xy} \end{Bmatrix}; \ \boldsymbol{\kappa}_2 = \begin{Bmatrix} \beta_{x,x} \\ \beta_{y,y} \\ \beta_{x,y} + \beta_{y,x} \end{Bmatrix}; \ \boldsymbol{\varepsilon}_s = \left\{\beta_x \quad \beta_y\right\}^T \end{aligned} \tag{7}$$

It is noted that $\boldsymbol{\varepsilon}_0^{NL}$ is the nonlinear components of in-plane, which can be rewritten in the following form:

$$\boldsymbol{\varepsilon}_0^{NL} = \frac{1}{2}\mathbf{A}_\theta\boldsymbol{\theta} = \begin{bmatrix} w_{0,x} & 0 \\ 0 & w_{0,y} \\ w_{0,y} & w_{0,x} \end{bmatrix}\begin{Bmatrix} w_{0,x} \\ w_{0,y} \end{Bmatrix} \tag{8}$$

The components of rotation vector θ_i associated with Eq. (5) are given by:

$$\begin{aligned}
\theta_x &= \frac{1}{2}\left(\frac{\partial w}{\partial y} - \frac{\partial v}{\partial z}\right) = \frac{1}{2}\left(2w_{0,y} - f'(z)\beta_y\right)\\
\theta_y &= \frac{1}{2}\left(\frac{\partial u}{\partial z} - \frac{\partial w}{\partial x}\right) = \frac{1}{2}\left(-2w_{0,x} + f'(z)\beta_x\right)\\
\theta_z &= \frac{1}{2}\left(\frac{\partial v}{\partial x} - \frac{\partial u}{\partial y}\right) = \frac{1}{2}\left(\left(v_{0,x} - u_{0,y}\right) + f(z)\left(\beta_{y,x} - \beta_{x,y}\right)\right)
\end{aligned} \tag{9}$$

And the components of curvature vector χ_{ij} are written in compact form as follows:

$$\begin{aligned}
\boldsymbol{\chi}^b &= \left\{\chi_x \quad \chi_y \quad \chi_{xy} \quad \chi_z\right\}^T = \boldsymbol{\chi}_1^b + f'(z)\boldsymbol{\chi}_2\\
\boldsymbol{\chi}^s &= \left\{\chi_{xz} \quad \chi_{yz}\right\}^T = \boldsymbol{\chi}_0^s + f(z)\boldsymbol{\chi}_1^s + f''(z)\boldsymbol{\chi}_2
\end{aligned} \tag{10}$$

where

$$\begin{aligned}
&\boldsymbol{\chi}_1^b = \frac{1}{2}\begin{Bmatrix} 2w_{0,xy} \\ 2w_{0,xy} \\ \left(w_{0,yy} - w_{0,xx}\right) \\ 0 \end{Bmatrix}; \boldsymbol{\chi}_2^b = \frac{1}{4}\begin{Bmatrix} -2\beta_{y,x} \\ 2\beta_{x,y} \\ \beta_{x,x} - \beta_{y,y} \\ 2\left(\beta_{y,x} - \beta_{x,y}\right) \end{Bmatrix}\\
&\boldsymbol{\chi}_0^s = \frac{1}{4}\begin{Bmatrix} v_{0,xx} - u_{0,xy} \\ v_{0,xy} - u_{0,yy} \end{Bmatrix}; \ \boldsymbol{\chi}_1^s = \frac{1}{4}\begin{Bmatrix} \beta_{y,xx} - \beta_{x,xy} \\ \beta_{y,xy} - \beta_{x,yy} \end{Bmatrix}; \ \boldsymbol{\chi}_2^s = \frac{1}{4}\begin{Bmatrix} -\beta_y \\ \beta_x \end{Bmatrix}
\end{aligned} \tag{11}$$

It is noted that, the subscripts ‘,x’ ‘,y’ represent the derivative of arbitrary function for x and y directions, respectively.

According to the MCST with one MLS parameter proposed by Yang et al. [13], the constitutive equation for the stress and strain tensor, respectively, are defined as:

$$\sigma_{ij} = C_{ijkl}\varepsilon_{kl} \tag{12}$$

$$m_{ij} = 2G\ell^2\chi_{ij} \tag{13}$$

where C_{ijkl} is the elasticity constant; G and ℓ are the shear module and the MLS parameter, respectively.

Furthermore, the CNTRC material behavior is similar to the orthotropic material. Nevertheless, in this work, the shear modulus of FG-CNTRC micro-plate in three directions are assumed to be equal, i.e. $G = G_{12} = G_{13} = G_{23}$. Therefore, the MCST can be applied to predict the small size-dependent effect of FG-CNTRC micro-plate.

Accordingly, the stress and couple stress-curvature constitutive relations associated with the MCST, respectively, are written as:

$$\begin{Bmatrix} \sigma_x \\ \sigma_y \\ \tau_{xy} \\ \tau_{xz} \\ \tau_{yz} \end{Bmatrix} = \begin{bmatrix} Q_{11} & Q_{12} & 0 & 0 & 0 \\ Q_{21} & Q_{22} & 0 & 0 & 0 \\ 0 & 0 & Q_{66} & 0 & 0 \\ 0 & 0 & 0 & Q_{55} & 0 \\ 0 & 0 & 0 & 0 & Q_{44} \end{bmatrix} \begin{Bmatrix} \varepsilon_x \\ \varepsilon_y \\ \gamma_{xy} \\ \gamma_{xz} \\ \gamma_{yz} \end{Bmatrix} \tag{14}$$

$$\begin{Bmatrix} m_x \\ m_y \\ m_{xy} \\ m_z \\ m_{xz} \\ m_{yz} \end{Bmatrix} = 2G\ell^2 \begin{bmatrix} 1 & 0 & 0 & 0 & 0 & 0 \\ 0 & 1 & 0 & 0 & 0 & 0 \\ 0 & 0 & 1 & 0 & 0 & 0 \\ 0 & 0 & 0 & 1 & 0 & 0 \\ 0 & 0 & 0 & 0 & 1 & 0 \\ 0 & 0 & 0 & 0 & 0 & 1 \end{bmatrix} \begin{Bmatrix} \chi_x \\ \chi_y \\ \chi_{xy} \\ \chi_z \\ \chi_{xz} \\ \chi_{yz} \end{Bmatrix} \tag{15}$$

where

$$Q_{11} = \frac{E_{11}}{1-\nu_{12}\nu_{21}},\; Q_{12} = Q_{21} = \frac{\nu_{12}E_{22}}{1-\nu_{12}\nu_{21}},\; Q_{22} = \frac{E_{22}}{1-\nu_{12}\nu_{21}},\; Q_{66} = G_{12},\; Q_{55} = G_{13},\; Q_{44} = G_{23} \tag{16}$$

in which, E_{11} and E_{22} are the Young's moduli of the CNTRC plates in the principal material coordinates, G_{12}, G_{13} and G_{23} are the effective shear moduli in the 1-2, 1-3 and 2-3 planes, respectively and $\nu_{21} = \left(E_{22}/E_{11}\right)\nu_{12}$ is Poisson's ratio.

Next, the in-plane forces, moments, higher order forces and shear forces are expressed as:

$$\begin{Bmatrix} N_{ij} \\ M_{ij} \\ P_{ij} \end{Bmatrix} = \int_{-h/2}^{h/2} \sigma_{ij} \begin{Bmatrix} 1 \\ z \\ f(z) \end{Bmatrix} \mathrm{d}z \quad ij := x,y$$
$$Q_{\alpha z} = \int_{-h/2}^{h/2} \tau_{\alpha z} f'(z) \mathrm{d}z \quad \alpha := x,y \tag{17}$$

From Eq. (5), (14), (17), the stress resultant can be expressed in matrix form as:

$$\hat{\boldsymbol{\sigma}} = \begin{Bmatrix} \mathbf{N}^u \\ \mathbf{M}^u \\ \mathbf{P}^u \\ \mathbf{Q}^u \end{Bmatrix} = \begin{bmatrix} \mathbf{A}^u & \mathbf{B}^u & \mathbf{E}^u & \mathbf{0} \\ \mathbf{B}^u & \mathbf{D}^u & \mathbf{F}^u & \mathbf{0} \\ \mathbf{E}^u & \mathbf{F}^u & \mathbf{H}^u & \mathbf{0} \\ \mathbf{0} & \mathbf{0} & \mathbf{0} & \mathbf{D}^{us} \end{bmatrix} \begin{Bmatrix} \boldsymbol{\varepsilon}_0 \\ \boldsymbol{\kappa}_1 \\ \boldsymbol{\kappa}_2 \\ \boldsymbol{\varepsilon}_s \end{Bmatrix} = \hat{\mathbf{D}}_u \hat{\boldsymbol{\varepsilon}} \tag{18}$$

in which

$$\left(\mathbf{A}^u,\mathbf{B}^u,\mathbf{D}^u,\mathbf{E}^u,\mathbf{F}^u,\mathbf{H}^u\right)=\int_{-h/2}^{h/2}\left(1,z,z^2,f(z),zf(z),[f(z)]^2\right)\begin{bmatrix} Q_{11} & Q_{12} & 0 \\ Q_{21} & Q_{22} & 0 \\ 0 & 0 & Q_{66} \end{bmatrix}\mathrm{d}z$$

$$\mathbf{D}^{us}=\int_{-h/2}^{h/2}\left[f'(z)\right]^2\begin{bmatrix} Q_{44} & 0 \\ 0 & Q_{55} \end{bmatrix}\mathrm{d}z \tag{19}$$

Similarly, from Eq. (10) and Eq. (15), the couple stress moment resultant is:

$$\hat{\mathbf{m}}=\begin{Bmatrix} \mathbf{N}^c \\ \mathbf{M}^c \\ \mathbf{Q}^c \\ \mathbf{R}^c \\ \mathbf{T}^c \end{Bmatrix}=\begin{bmatrix} \mathbf{A}^c & \mathbf{B}^c & \mathbf{0} & \mathbf{0} & \mathbf{0} \\ \mathbf{B}^c & \mathbf{E}^c & \mathbf{0} & \mathbf{0} & \mathbf{0} \\ \mathbf{0} & \mathbf{0} & \mathbf{X}^c & \mathbf{Y}^c & \mathbf{T}^c \\ \mathbf{0} & \mathbf{0} & \mathbf{Y}^c & \mathbf{Z}^c & \mathbf{V}^c \\ \mathbf{0} & \mathbf{0} & \mathbf{T}^c & \mathbf{V}^c & \mathbf{W}^c \end{bmatrix}\begin{Bmatrix} \boldsymbol{\chi}_1^b \\ \boldsymbol{\chi}_2^b \\ \boldsymbol{\chi}_0^s \\ \boldsymbol{\chi}_1^s \\ \boldsymbol{\chi}_2^s \end{Bmatrix}=\hat{\mathbf{D}}_c\hat{\boldsymbol{\chi}} \tag{20}$$

in which

$$\left(\mathbf{A}^c,\mathbf{B}^c,\mathbf{E}^c\right)=\int_{-h/2}^{h/2}\left(1,f'(z),[f'(z)]^2\right)\begin{bmatrix} 2G\ell^2 & 0 & 0 & 0 \\ 0 & 2G\ell^2 & 0 & 0 \\ 0 & 0 & 2G\ell^2 & 0 \\ 0 & 0 & 0 & 2G\ell^2 \end{bmatrix}\mathrm{d}z$$

$$(\mathbf{X}^c,\mathbf{Y}^c,\mathbf{Z}^c,\mathbf{T}^c,\mathbf{V}^c,\mathbf{W}^c)=\int_{-h/2}^{h/2}\left(1,f(z),[f(z)]^2,f''(z),f(z)f''(z),[f''(z)]^2\right)\begin{bmatrix} 2G\ell^2 & 0 \\ 0 & 2G\ell^2 \end{bmatrix}\mathrm{d}z \tag{21}$$

As a result, the virtual strain energy of FG-CNTRC micro-plate using MCST is now established as follows

$$\delta U=\int_\Omega(\hat{\boldsymbol{\sigma}}\delta\hat{\boldsymbol{\varepsilon}}+\hat{\mathbf{m}}\delta\hat{\boldsymbol{\chi}})\mathrm{d}\Omega \tag{22}$$

By using the principle of virtual displacement, the discrete Galerkin weak form for nonlinear responses of FG-CNTRC micro-plate subjected to uniform loading q can be established such as:

$$\int_\Omega\delta\hat{\boldsymbol{\varepsilon}}^{\mathrm{T}}\hat{\mathbf{D}}_u\hat{\boldsymbol{\varepsilon}}\mathrm{d}\Omega+\int_\Omega\delta\hat{\boldsymbol{\chi}}^{\mathrm{T}}\hat{\mathbf{D}}_c diag\left(\boldsymbol{\Gamma}_\chi\right)\hat{\boldsymbol{\chi}}\mathrm{d}\Omega+\int_\Omega\delta\dot{\mathbf{u}}^T\mathbf{m}\ddot{\mathbf{u}}\mathrm{d}\Omega=\int_\Omega\delta wq\mathrm{d}\Omega \tag{23}$$

in which, $diag\left(\boldsymbol{\Gamma}_\chi\right)=diag\left(1,\ 1,\ 2,1,1,1\right)$ is the diagonal matrix.

Besides, the last term in left hand side of Eq. (23) is computed by:

$$\begin{aligned}\int_\Omega \delta\dot{\tilde{\mathbf{u}}}^T \mathbf{m}\dot{\tilde{\mathbf{u}}}\,\mathrm{d}\Omega &= \int_\Omega\int_{-h/2}^{h/2}\rho\left(\dot{u}\delta\dot{u}+\dot{v}\delta\dot{v}+\dot{w}\delta\dot{w}\right)\mathrm{d}x\mathrm{d}y\mathrm{d}z\\ &= \int_\Omega\int_{-h/2}^{h/2}\rho\Big[\left(\dot{u}_0 - z\dot{w}_{0,x}+f(z)\dot{\beta}_x\right)\left(\delta\dot{u}_0 - z\delta\dot{w}_{0,x}+f(z)\delta\dot{\beta}_x\right)+\\ &\qquad\left(\dot{v}_0 - z\dot{w}_{0,y}+f(z)\dot{\beta}_y\right)\left(\delta\dot{v}_0 - z\delta\dot{w}_{0,y}+f(z)\delta\dot{\beta}_y\right)+\dot{w}_0\delta\dot{w}_0\Big]\mathrm{d}x\mathrm{d}y\mathrm{d}z\\ &= \int_\Omega\left(\left(\delta\dot{\mathbf{u}}_1\right)^T\mathbf{I}_0\dot{\mathbf{u}}_1+\left(\delta\dot{\mathbf{u}}_2\right)^T\mathbf{I}_0\dot{\mathbf{u}}_2+\left(\delta\dot{\mathbf{u}}_3\right)^T\mathbf{I}_0\dot{\mathbf{u}}_3\right)\mathrm{d}\Omega\end{aligned} \tag{24}$$

in which $\tilde{\mathbf{u}}=\{\mathbf{u}_1\quad\mathbf{u}_2\quad\mathbf{u}_3\}^T$, $\mathbf{u}_1=\{u_0\quad -w_{,x}\quad \beta_x\}^T$, $\mathbf{u}_2=\{v_0\quad -w_{,y}\quad \beta_y\}^T$, $\mathbf{u}_3=\{w_0\quad 0\quad 0\}^T$, ρ are the mass density per unit volume; $\mathbf{m}$ is the mass matrix that is expressed as follows

$$\mathbf{m}=\begin{bmatrix}\mathbf{I}_0 & 0 & 0\\ 0 & \mathbf{I}_0 & 0\\ 0 & 0 & \mathbf{I}_0\end{bmatrix};\ \mathbf{I}_0=\begin{bmatrix}I_1 & I_2 & I_4\\ I_2 & I_3 & I_5\\ I_4 & I_5 & I_6\end{bmatrix};\ \left(I_1,I_2,I_3,I_4,I_5,I_6\right)=\int_{-h/2}^{h/2}\rho\left(1,z,z^2,f(z),zf(z),\left(f(z)\right)^2\right)\mathrm{d}z \tag{25}$$

3. FG-CNTRC micro-plate based on NURBS basis function

3.1. Brief of isogeometric analysis

In 1D, the B-spline basis function is a piecewise polynomial of degree p that is recursively constructed by Cox-De Boor algorithm as follow:

$$p = 0,\ N_{i,0}(\xi)=\begin{cases}1 & \text{if } \xi_i \le \xi < \xi_{i+1}\\ 0 & \text{otherwise}\end{cases} \tag{26}$$

$$p \ge 1,\ N_{i,p}(\xi)=\frac{\xi-\xi_i}{\xi_{i+p}-\xi_i}N_{i,p-1}(\xi)+\frac{\xi_{i+p+1}-\xi}{\xi_{i+p+1}-\xi_{i+1}}N_{i+1,p-1}(\xi)$$

where $\xi_i \in R$ is called knot and, $i=1,2,...,n+p+1$ is knot index, p is the order of polynomial function and n is the number of basic function; The value of knot is taken from the knot vector $\Xi=\left\{\xi_1,\xi_2,...,\xi_{n+p+1}\right\}$. If two end knots are repeated $p+1$ times the knot vector is open. As seen in Fig. 3, the one-dimensional (1D) quadratic B-spline basic functions for an open knot are plotted.

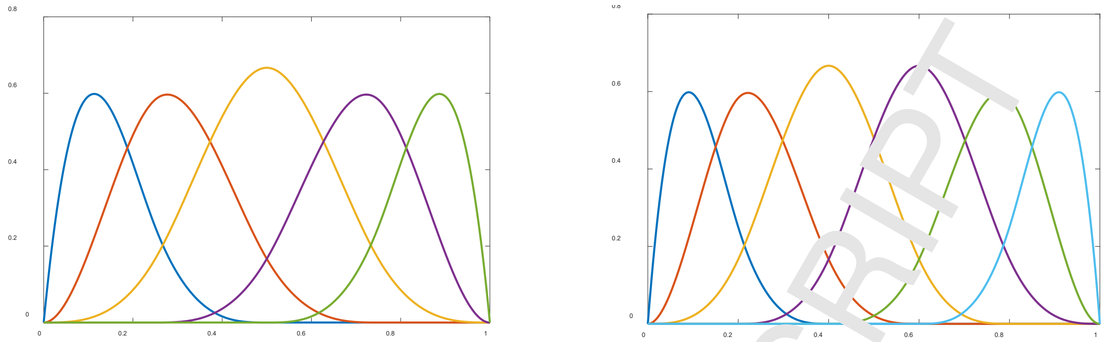

$\Xi = \{0,\ 0,\ 0,\ 0.25,\ 0.5,\ 0.75,\ 1,\ 1,\ 1\}$ $\quad$ $\mathrm{H} = \{0,\ 0,\ 0,\ 0.2,\ 0.4,\ 0.6,\ 0.8,\ 1,\ 1,\ 1\}$

Fig. 3. Quadratic B-spline basic functions.

The non-uniform rational basis spline (NURBS) basis functions is constructed based on a tensor product of two 1D B-splines with polynomial degrees of p and q such as:

$$\mathrm{X}(\xi,\eta) = \frac{N_i^p(\xi)M_j^q(\eta)w_{ij}}{\sum_{i=1}^{n}\sum_{j=1}^{m} N_i^p(\xi)M_j^q(\eta)w_{ij}} \tag{27}$$

in which w_{ij} is the control weight.

3.2. NURBS-based formulation of FG-CNTRC

Based on isogeometric analysis, this study establishes a suitable numerical model that easily fulfill higher-order derivative requirement in discrete Galerkin weak form. Herein, the NURBS basis function is employed to build a finite approximation of displacement field in following form [54, 75, 76]:

$$\mathbf{u}^h = \begin{Bmatrix} u_0 \\ v_0 \\ w_0 \\ \beta_x \\ \beta_y \end{Bmatrix} = \sum_{I=1}^{mxn} \begin{bmatrix} N_I & 0 & 0 & 0 & 0 \\ 0 & N_I & 0 & 0 & 0 \\ 0 & 0 & N_I & 0 & 0 \\ 0 & 0 & 0 & N_I & 0 \\ 0 & 0 & 0 & 0 & N_I \end{bmatrix} \begin{Bmatrix} u_{0I} \\ v_{0I} \\ w_{0I} \\ \beta_{xI} \\ \beta_{yI} \end{Bmatrix} = \sum_{I=1}^{mxn} \mathbf{N}_I \mathbf{d}_I \tag{28}$$

where $\mathbf{d}_I = \{u_{0I} \quad v_{0I} \quad w_{0I} \quad \beta_{xI} \quad \beta_{yI}\}^T$, $\mathbf{N}_I$, respectively, are the vector of degree of freedoms associated with the control point I and the shape function.

Replacing Eq. (28) into Eq. (7), the strain components is now expressed in matrix form as:

$$\hat{\boldsymbol{\varepsilon}} = \sum_{i=1}^{m\times n}\left(\mathbf{B}_I^L + \frac{1}{2}\mathbf{B}_I^{NL}\right)\mathbf{d}_I \tag{29}$$

where $\mathbf{B}_I^L = \left[\left(\mathbf{B}_I^m\right)^T \quad \left(\mathbf{B}_I^{b1}\right)^T \quad \left(\mathbf{B}_I^{b2}\right)^T \quad \left(\mathbf{B}_I^s\right)^T\right]^T$, in which

$$\mathbf{B}_I^m = \begin{bmatrix} N_{I,x} & 0 & 0 & 0 & 0 \\ 0 & N_{I,y} & 0 & 0 & 0 \\ N_{I,y} & N_{I,x} & 0 & 0 & 0 \end{bmatrix}; \mathbf{B}_I^{b1} = -\begin{bmatrix} 0 & 0 & N_{I,xx} & 0 & 0 \\ 0 & 0 & N_{I,yy} & 0 & 0 \\ 0 & 0 & 2N_{I,xy} & 0 & 0 \end{bmatrix}; \mathbf{B}_I^{b2} = \begin{bmatrix} 0 & 0 & 0 & N_{I,x} & 0 \\ 0 & 0 & 0 & 0 & N_{I,y} \\ 0 & 0 & 0 & N_{I,y} & N_{I,x} \end{bmatrix};$$
$$\mathbf{B}_I^s = \begin{bmatrix} 0 & 0 & 0 & N_I & 0 \\ 0 & 0 & 0 & 0 & N_I \end{bmatrix} \tag{30}$$
$$\mathbf{B}_I^{NL}\left(\mathbf{d}\right) = \begin{bmatrix} \mathbf{A}_\theta \\ \mathbf{0} \end{bmatrix}\mathbf{B}_I^g \text{ with } \mathbf{B}_I^g = \begin{bmatrix} 0 & 0 & N_{I,x} & 0 & 0 \\ 0 & 0 & N_{I,y} & 0 & 0 \end{bmatrix}$$

Substituting Eq. (28) into Eq. (11), the couple stress curvature components are rewritten in matrix form as:

$$\hat{\boldsymbol{\chi}} = \sum_{i=1}^{m\times n}\mathbf{B}_I^\chi \mathbf{d}_I \text{ where } \mathbf{B}_I^\chi = \left[\left(\boldsymbol{\chi}_1^b\right)^T \quad \left(\boldsymbol{\chi}_2^b\right)^T \quad \left(\boldsymbol{\chi}_0^s\right)^T \quad \left(\boldsymbol{\chi}_1^s\right)^T \quad \left(\boldsymbol{\chi}_2^s\right)^T\right]^T \tag{31}$$

in which

$$\mathbf{B}_I^{\chi b1} = \frac{1}{2}\begin{bmatrix} 0 & 0 & 2N_{I,xy} & 0 & 0 \\ 0 & 0 & -2N_{I,xy} & 0 & 0 \\ 0 & 0 & \left(N_{I,yy} - N_{I,xx}\right) & 0 & 0 \\ 0 & 0 & 0 & 0 & 0 \end{bmatrix}; \mathbf{B}_I^{\chi b2} = \frac{1}{4}\begin{bmatrix} 0 & 0 & 0 & 0 & -2N_{I,x} \\ 0 & 0 & 0 & 2N_{I,y} & 0 \\ 0 & 0 & 0 & N_{I,x} & -N_{I,y} \\ 0 & 0 & 0 & -2N_{I,y} & 2N_{I,x} \end{bmatrix}$$
$$\mathbf{B}_I^{\chi s0} = \frac{1}{4}\begin{bmatrix} -N_{I,xy} & N_{I,xx} & 0 & 0 & 0 \\ -N_{I,yy} & N_{I,xy} & 0 & 0 & 0 \end{bmatrix}; \quad \mathbf{B}_I^{\chi s1} = \frac{1}{4}\begin{bmatrix} 0 & 0 & 0 & -N_{I,xy} & N_{I,xx} \\ 0 & 0 & 0 & -N_{I,yy} & N_{I,xy} \end{bmatrix} \tag{32}$$
$$\mathbf{B}_I^{\chi s2} = \frac{1}{4}\begin{bmatrix} 0 & 0 & 0 & 0 & -N_I \\ 0 & 0 & 0 & N_I & 0 \end{bmatrix}$$

Substituting Eq. (29) and Eq. (31) into Eq. (23), the virtual displacement vector $\delta\mathbf{d}$ is eliminated and the global equation of motion of FG-CNTRC micro-plate is established in the matrix form as follows:

$$\left(\mathbf{K}_L + \mathbf{K}_{NL}\right)\mathbf{d} + \mathbf{M}\ddot{\mathbf{d}} = \mathbf{F} \tag{33}$$

where $\mathbf{K}_L = \mathbf{K}_L^u + \mathbf{K}_L^\theta$ and $\mathbf{K}_{NL}$, respectively, are the linear and nonlinear global stiffness matrix and $\mathbf{M}$ is the global mass matrix. These matrices are expressed in a clear form as:

$$\mathbf{K}_L^u = \int_\Omega \left(\mathbf{B}^L\right)^T \hat{\mathbf{D}}_u \mathbf{B}^L \mathrm{d}\Omega$$
$$\mathbf{K}_L^\theta = \int_\Omega \left(\mathbf{B}^\chi\right)^T \hat{\mathbf{D}}_c \mathbf{B}^\chi \mathrm{d}\Omega$$
$$\mathbf{K}_{NL} = \frac{1}{2}\int_\Omega \left(\mathbf{B}^L\right)^T \hat{\mathbf{D}}_u \mathbf{B}^{NL} \mathrm{d}\Omega + \int_\Omega \left(\mathbf{B}^{NL}\right)^T \hat{\mathbf{D}}_u \mathbf{B}^L \mathrm{d}\Omega + \frac{1}{2}\int_\Omega \left(\mathbf{B}^{NL}\right)^T \hat{\mathbf{D}}_u \mathbf{B}^{NL} \mathrm{d}\Omega \tag{34}$$
$$\mathbf{M} = \int_\Omega \tilde{\mathbf{R}}^T \mathbf{m} \tilde{\mathbf{R}} \mathrm{d}\Omega$$

where

$$\tilde{\mathbf{R}} = \begin{Bmatrix} \mathbf{R}_1 \\ \mathbf{R}_2 \\ \mathbf{R}_3 \end{Bmatrix}; \quad \mathbf{R}_1 = \begin{bmatrix} N_I & 0 & 0 & 0 & 0 \\ 0 & 0 & -N_{I,x} & 0 & 0 \\ 0 & 0 & 0 & N_I & 0 \end{bmatrix};$$
$$\mathbf{R}_2 = \begin{bmatrix} 0 & N_I & 0 & 0 & 0 \\ 0 & 0 & -N_{I,y} & 0 & 0 \\ 0 & 0 & 0 & 0 & N_I \end{bmatrix}; \quad \mathbf{R}_3 = \begin{bmatrix} 0 & 0 & N_I & 0 & 0 \\ 0 & 0 & 0 & 0 & 0 \\ 0 & 0 & 0 & 0 & 0 \end{bmatrix} \tag{35}$$

In the following equation, the external force vector is given by:

$$\mathbf{F} = \int_\Omega q(t)\begin{bmatrix} 0 & 0 & N_I & 0 & 0 \end{bmatrix}^T \mathrm{d}\Omega \tag{36}$$

In addition, the structural damping of FG-CNTRC micro-plate is derived through Rayleigh damping. Thus, the nonlinear equation of motion in Eq. (33) is now rewritten in the following matrix form:

$$\mathbf{Kd} + \mathbf{C}\dot{\mathbf{d}} + \mathbf{M}\ddot{\mathbf{d}} = \mathbf{F} \tag{37}$$

where $\mathbf{K} = \mathbf{K}_L + \mathbf{K}_{NL}$ and the structural damping matrix $\mathbf{C}$ is defined based on a linear association between $\mathbf{K}$ and $\mathbf{M}$ such as:

$$\mathbf{C} = \gamma_R \mathbf{M} + \varsigma_R \mathbf{K} \tag{38}$$

in which the Rayleigh damping coefficients $(\gamma_R,\ \varsigma_R)$ are obtained from the experimental work. However, in this study, γ_R and ς_R are defined as in Ref. [77], where a damping ratio of FG-CNTRC plate was assumed to be 0.3.

4. Nonlinear solution procedure

4.1 Nonlinear static bending solution

In this study, the nonlinear static equation $\left(\mathbf{K}_L + \mathbf{K}_{NL}\right)\mathbf{d} = \mathbf{F}$ is obtained by neglecting the mass matrix effect in Eq. (33) that is solved by using Newton-Raphson technique. At a specific load level m^{th}, the residual force $\mathbf{R}(\mathbf{d}^i)$ at i^{th} iteration is computed as follows:

$$\mathbf{R}\left(\mathbf{d}^i\right) = \left(\mathbf{K}_L + \mathbf{K}_{NL}\left(\mathbf{d}^i\right)\right) - \mathbf{F}^m \tag{39}$$

By iterations, the residual force tends to zero. When the residual force is still large enough, the displacement at $(i+1)^{\text{th}}$ iteration, is then calculated as:

$$\mathbf{d}^{i+1} = \mathbf{d}^i + \Delta\mathbf{d}^{i+1} \tag{40}$$

The increment displacement $\Delta\mathbf{d}^{i+1}$ is computed by following equation:

$$\Delta\mathbf{d}^{i+1} = -\mathbf{R}\left(\mathbf{d}^i\right) \big/ \mathbf{K}_T\left(\mathbf{d}_i\right) \tag{41}$$

where the tangent stiffness matrix $\mathbf{K}_T$ at i^{th} iteration is defined as:

$$\mathbf{K}_T\left(\mathbf{d}^i\right) = \frac{\partial \mathbf{R}\left(\mathbf{d}^i\right)}{\partial \mathbf{d}^i} = \tilde{\mathbf{K}}_{NL} + \mathbf{K}_g \tag{42}$$

in which the stiffness matrix $\tilde{\mathbf{K}}_{NL}$ contains the variables $\mathbf{d}_i$ given by:

$$\tilde{\mathbf{K}}_{NL} = \int_\Omega \left(\mathbf{B}^L + \mathbf{B}^{NL}\right)^T \hat{\mathbf{D}}_u \left(\mathbf{B}^L + \mathbf{B}^{NL}\right) \mathrm{d}\Omega + \int_\Omega \left(\mathbf{B}^\chi\right)^T \hat{\mathbf{D}}_c \mathbf{B}^\chi \mathrm{d}\Omega \tag{43}$$

And $\mathbf{K}_g$ is the geometric stiffness matrix that related to the in-plane forces and is defined such as

$$\mathbf{K}_g = \int_\Omega \left(\mathbf{B}^g\right)^T \begin{bmatrix} N_x^0 & N_{xy}^0 \\ N_{xy}^0 & N_y^0 \end{bmatrix} \left(\mathbf{B}^g\right) \mathrm{d}\Omega \tag{44}$$

The iteration is repeated until the convergence condition of displacement is obtained. In other words, the displacement error between two uninterrupted iterations must be smaller than an allowable error, i.e.:

$$\frac{\left\|\mathbf{d}^{i+1} - \mathbf{d}^i\right\|}{\left\|\mathbf{d}^i\right\|} < 0.01 \tag{45}$$

4.2 Nonlinear dynamic solution

In this section, the Newmark's integration procedure with the average acceleration method [77] is utilized to obtain the solution of the equation of dynamic system in Eq. (33) and Eq. (37). Additionally, the nonlinear responses of plate are obtained by using the Picard method. Specifically, at the initial time step $t = 0$, the displacement, velocity and acceleration are assumed to be zeros. As the displacement $\mathbf{d}$ is found at time $t = (n + 1)\Delta t$, the velocity and acceleration are calculated as follows:

$$\ddot{\mathbf{d}}_{n+1} = \frac{1}{\beta\Delta t^2}\left(\mathbf{d}_{n+1} - \mathbf{d}_n\right) - \frac{1}{\beta\Delta t^2}\dot{\mathbf{d}}_n - \left(\frac{1}{2\beta} - 1\right)\ddot{\mathbf{d}}_n \tag{46}$$

$$\dot{\mathbf{d}}_{n+1} = \dot{\mathbf{d}}_n + \Delta t\left(1-\gamma\right)\ddot{\mathbf{d}}_n + \gamma\Delta t\ddot{\mathbf{d}}_{n+1} \tag{47}$$

in which, the Newmark $\beta = 1/4$ is known as the constant average acceleration method with the factor $\gamma = 1/2$. Substituting Eq. (46) and Eq. (47) into Eq. (37), the equation of motion is now rewritten as:

$$\hat{\mathbf{K}}_{n+1}\mathbf{d}_{n+1} = \hat{\mathbf{F}}_{n+1} \tag{48}$$

where $\hat{\mathbf{K}}_{n+1}$ is the effective stiffness matrix at time $(n + 1)\Delta t$

$$\hat{\mathbf{K}}_{n+1} = \mathbf{K}_{n+1} + \frac{1}{\beta\Delta t^2}\mathbf{M} + \frac{\gamma}{\beta\Delta t}\mathbf{C} \tag{49}$$

and the effective force vector

$$\hat{\mathbf{F}}_{n+1} = \mathbf{F}_{n+1} + \mathbf{M}\left[\frac{1}{\beta\Delta t^2}\mathbf{d}_n + \frac{1}{\beta\Delta t}\dot{\mathbf{d}}_n + \left(\frac{1}{2\beta} - 1\right)\ddot{\mathbf{d}}_n\right] + \mathbf{C}\left[\frac{\gamma}{\beta\Delta t}\mathbf{d}_n + \left(\frac{\gamma}{\beta} - 1\right)\dot{\mathbf{d}}_n + \frac{\Delta t}{2}\left(\frac{\gamma}{\beta} - 2\right)\ddot{\mathbf{d}}_n\right] \tag{50}$$

It is noted that in Eq. (49) and Eq. (50), all parameters are found at previous step, i.e. $t = n\Delta t$. However, the nonlinear stiffness matrix $\mathbf{K}_{n+1}$ is dependent on the displacement at $t = (n + 1)\Delta t$. In this way, the Picard is assigned to re-approximate Eq. (48) such as:

$$\hat{\mathbf{K}}\left(\mathbf{d}_{n+1}^{i}\right)\mathbf{d}_{n+1}^{i+1} + \hat{\mathbf{F}}_{n+1} \tag{51}$$

where the superscript 'i' represents the iteration number. Thus, Eq. (48) is iteratively solved until the convergence condition of displacement in Eq. (45) is satisfied.

In this article, the order of NURBS functions is $p = q = 3$. The numerical integration in IGA is same as in FEM, which is performed by the Gauss-Legendre quadrature. However, it is a more complex implementation in case of IGA. Integral over the entire geometry (in physical system) is split into integral over each physical element Ωe. The integral is pulled back to parametric element via the geometry mapping. Then, the integral over the parametric element is pulled back to the parent domain. Additionally, $(p + 1) \times (q + 1)$ are the number of Gaussian points that are adopted for two-dimensional element by using p^{th} and q^{th} orders NURBS

5. Results and discussions

In this section, several numerical investigations are investigated in order to show the small size-dependent effect on the nonlinear static and dynamic behaviors of FG-CNTRC micro-plate for different boundary conditions. Firstly, the accuracy of the presented model is authenticated by comparison with other published model in the literature. The Newton-Raphson iterative procedure in section 4.1 is employed to get the solutions of nonlinear static analysis. Afterward, the difference between nonlinear classical model and non-classical model (MCST) is explore through the change of material length scale parameter. Then, the Newmark Beta method is assigned to obtain the geometrical nonlinear dynamic response of FG-CNTRC micro-plate under excitation load. Moreover, the effect of microstructure size-dependent on dynamic analysis is also carefully studied. In this paper, the material properties of FG-CNTRC are determined as follows:

- The isotropic matrix (PmPV) at room temperature (T = 300 K) [67]

  $E^m = 2.1$ GPa , $\nu^m = 0.34$, $\rho^m = 1150$ kg/m^3
- The (10,10) SWCNTs [78]

$E_{11}^{CNT} = 5.6466$ TPa, $E_{22}^{CNT} = 7.08$ TPa, $G_{12}^{CNT} = 1.9445$ TPa, $\upsilon_{12}^{CNT} = 0.175$, $\rho^{CNT} = 1400$ kg/cm^3

In addition, the two boundary conditions (BC) in this study are:

- Simply support with movable edge (SSSS)

$$\begin{cases} v_0 = w_0 = \beta_y = 0 & \text{at left and right edges} \\ u_0 = w_0 = \beta_x = 0 & \text{at lower and upper edges} \end{cases}$$

- Clamped support (CCCC)

$$v = u = w = 0 \quad \text{at all edges}$$

5.1. Nonlinear static analysis

In order to validate the faithfulness and efficacy of the proposed nonlinear numerical solution, let us investigate the nonlinear static bending of FG-CNTRC square micro-plate under transverse uniform distributed load based on classical model $(\ell/h=0)$. The obtained non-dimensionless central deflection $\overline{w}=w/h$ versus load parameter $\overline{q}=q_0L^4/\left(E_mh^4\right)$ of SCSS and CCCC FG-CNTRC plates $(L/h=100)$ for different volume fraction $\left(V_{CNT}^{*}=0.11,\ 0.14,\ 0.17\right)$ are compared with those obtained by the element-free IMLS-Ritz of Zhang et al. [79] and are illustrated in Figs. 3-5. It can be seen that, the present nonlinear results for FG-O distribution are in good agreement with those of reference solution. Nevertheless, the nonlinear deflections derived from the proposed solution are slightly higher than those of reference solution for FG-V, UD, FG-X. Therefore, the proposed model will be utilized to predict the nonlinear static problem in following examples. It is clear that the linear stiffness matrix $\mathbf{K}_L$ is constant and Figs. 3 to 5 show the difference between linear and nonlinear analyses.

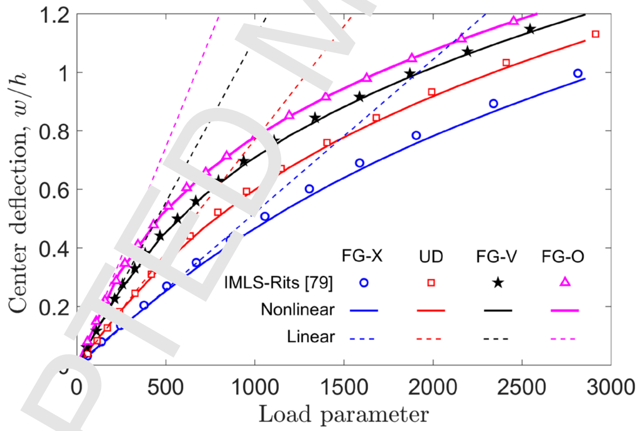

Fig. 3. Nonlinear deflection of clamped FG-CNTRC plate with different CNT distribution (L/h=100, $V_{CNT}^{*}=0.11$)

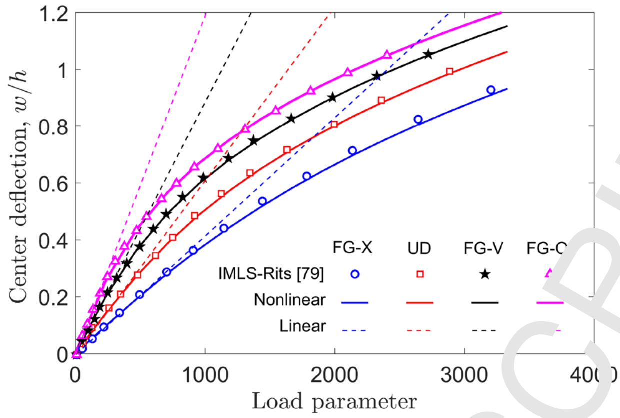

Fig. 4. Nonlinear deflection of clamped FG-CNTRC with different CNT distribution (L/h=100, $V_{CNT}^{*}=0.14$)

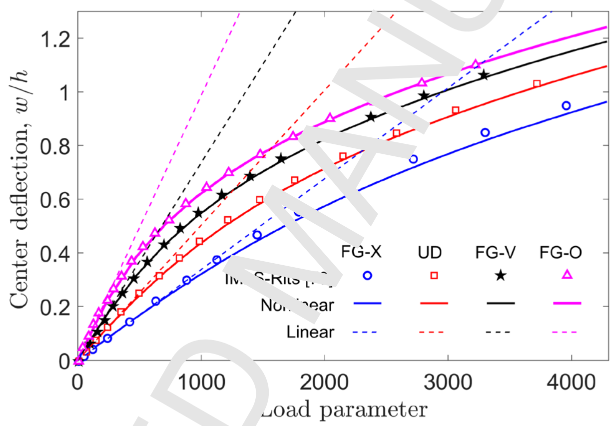

Fig. 5. Nonlinear deflection of clamped FG-CNTRC with different CNT distribution (L/h=100, $V_{CNT}^{*}=0.17$)

In order to show the reliability of the proposed solution in capturing the small size-dependent effect, a square FG micro-plate (L/h = 20, E_t = 14.4 GPa, E_b = 1.44 GPa, $\nu_t = \nu_b$ = 0.38) subjected to uniform distributed load using MCST is studied. The notations t and b denote the top and bottom surfaces and the nonlinear deflection curves are obtained after 20 load levels to reach $q_z = 5.4\times10^6$ N/m^2. As depicted in Fig. 6, there is a good agreement between the obtained results of homogeneous micro-plate and those from general third-order plate theory in Ref. [80] for various material length scale ratio ℓ/h = 0, 0.5 and 1.

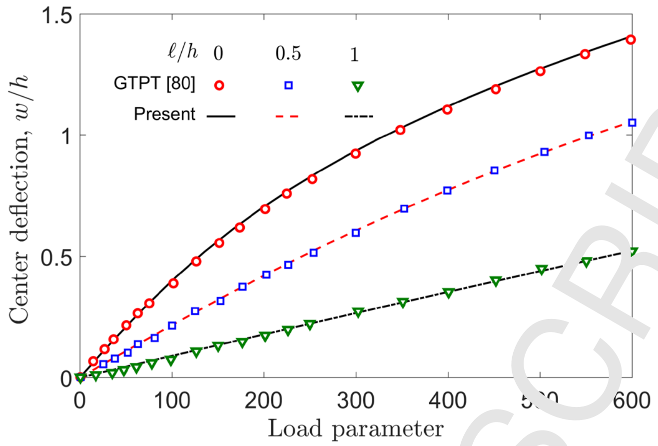

Fig. 6. Comparison between nonlinear deflection curves of homogeneous square micro-plate for various material length scale ratio ℓ/h

Next, a detailed study of the parametric effects of MLS parameter, CNT volume fraction, CNT distribution on the nonlinear deflection responses of FG-CNTRC micro-plates $(L/h = 10)$ is carried out in Figs. 7-12. It is worth mentioning that when ℓ/h varies from 0 to 1, $\ell/h = 0$ denotes the classical theory. Figs. 7-10 illustrate the influence of small size-dependent on the nonlinear deflection of FG-X, UD, FG-V and FG-O CNT reinforced composite micro-plate with the CNT volume fraction $V_{CNT}^{*} = 0.11$. It can be observed that the deflections are smaller for the higher value of length scale ratio ℓ/h. At the same load parameter level, the highest deflection is obtained for $\ell/h = 1$. Moreover, the deviation between classical and MCST model for CCCC BC as the ratio $\ell/h \leq 0.25$ is not noticeable, in spite of this the reduction of central deformation is remarkable as the ratio $\ell/h > 0.25$. It is also seen that an increase in ratio ℓ/h lead to decrease in nonlinear central deflection of FG-CNTRC micro-plate not only for SSSS but also for CCCC boundary condition, and this is because of the stiffness increase due to the size-dependent effect as $\ell/h \neq 0$.

In addition, the variation in central deflection with load parameter for UD and the other three patterns of CNTs distribution subjected a uniform transverse load are carried out in Fig. (10). It is clearly seen that the deflection responses of FG-O and FG-V are higher than those of UD and FG-X model. Besides, the minimum and maximum values of normalized central deflections are derived from FG-X and FG-O model, respectively. This is explained by a more significant increase in the stiffness of FG-CNT reinforced plate that is obtained at the top and bottom surfaces with CNT-rich compared to CNTs reinforced near the mid-plate. Furthermore, it is attained that the

MCST produces lower load-deflection curves more than classical theory $(\ell/h=0)$ due to stiffer stiffness of micro-plate for the length scale ratio $\ell/h \neq 0$. It is also observed from the figure that the nonlinear deflections of CCCC micro-plate are lower than those of the SSSS micro-plate. This is owning to the CCCC BC, which has less constraints compared to SSSS BC.

Fig. 12 reveals the influence of different volume fraction V_{CNT}^{*} on the load versus deflection curves of FG-CNTRC micro-plate for four patterns of CNTs distribution and the ratio $\ell/h=0,\ 1$. It can be seen that the volume fraction V_{CNT}^{*} increases from 0.11 to 0.17 leading to decrease in deflection. This behavior owning to the fact that there is an augmentation in CNTs reinforced in the isotropic matrix as CNTs volume fraction increases.

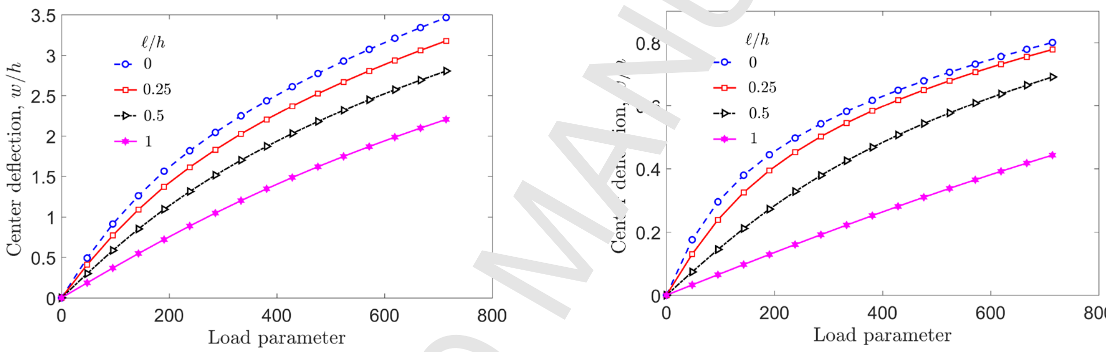

Fig. 7. Comparison of the load-deflection curve of FG-X micro-plate with $V_{CNT}^{*}=0.11$ and under: SSSS (left) and CCCC (right) boundary condition.

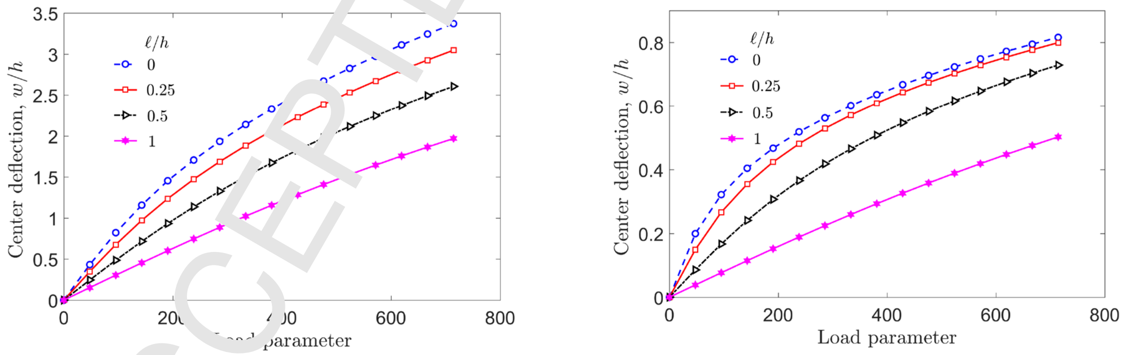

Fig. 8. Comparison of the load-deflection curve of UD micro-plate with $V_{CNT}^{*}=0.11$ under: SSSS (left) and CCCC (right) boundary condition.

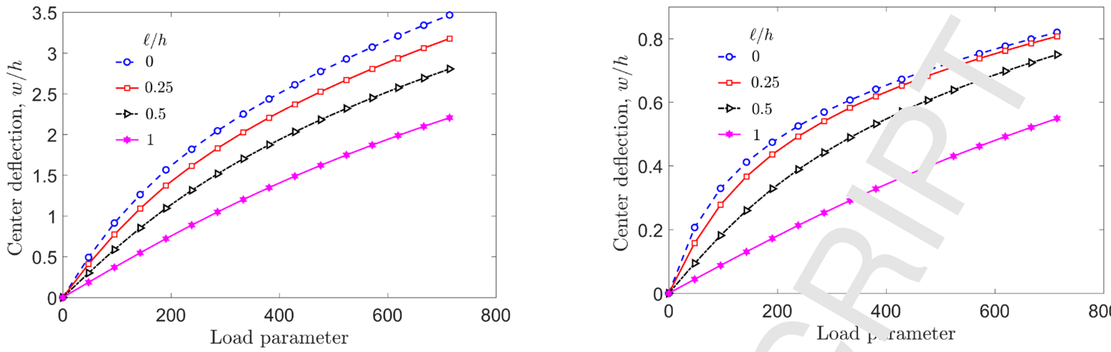

Fig. 9. Comparison of the load-deflection curve of FG-V micro-plate with $V_{CNT}^{*} = 0.11$ under: SSSS (left) and CCCC (right) boundary condition.

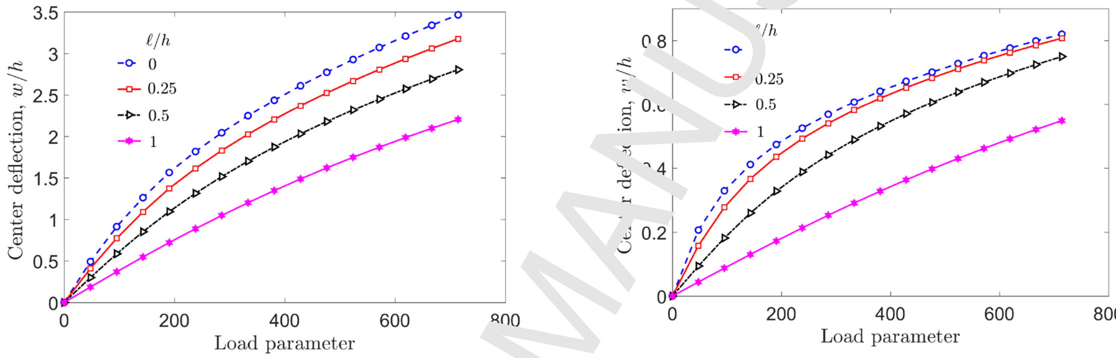

Fig. 10. Comparison of the load-deflection curve of FG-O micro-plate with $V_{CNT}^{*} = 0.11$ under: SSSS (left) and CCCC (right) boundary condition.

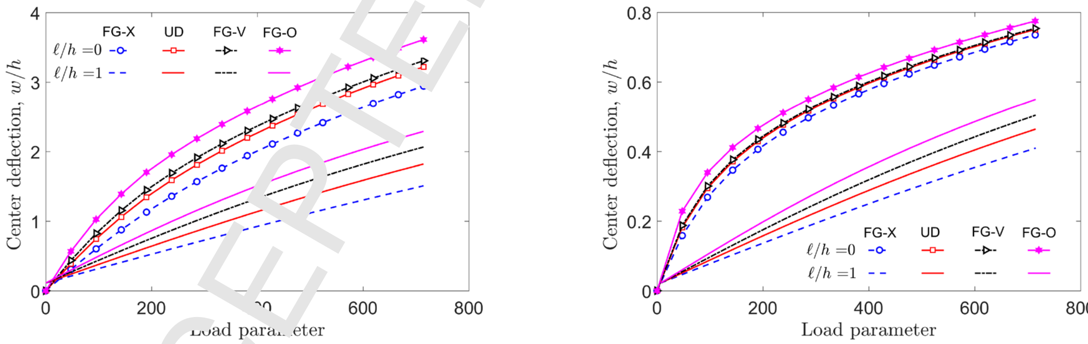

Fig. 11. Load-deflection curve of CNT micro-plate with $V_{CNT}^{*} = 0.14$ for the classical and MCST model under: SSSS (left) and CCCC (right) boundary condition.

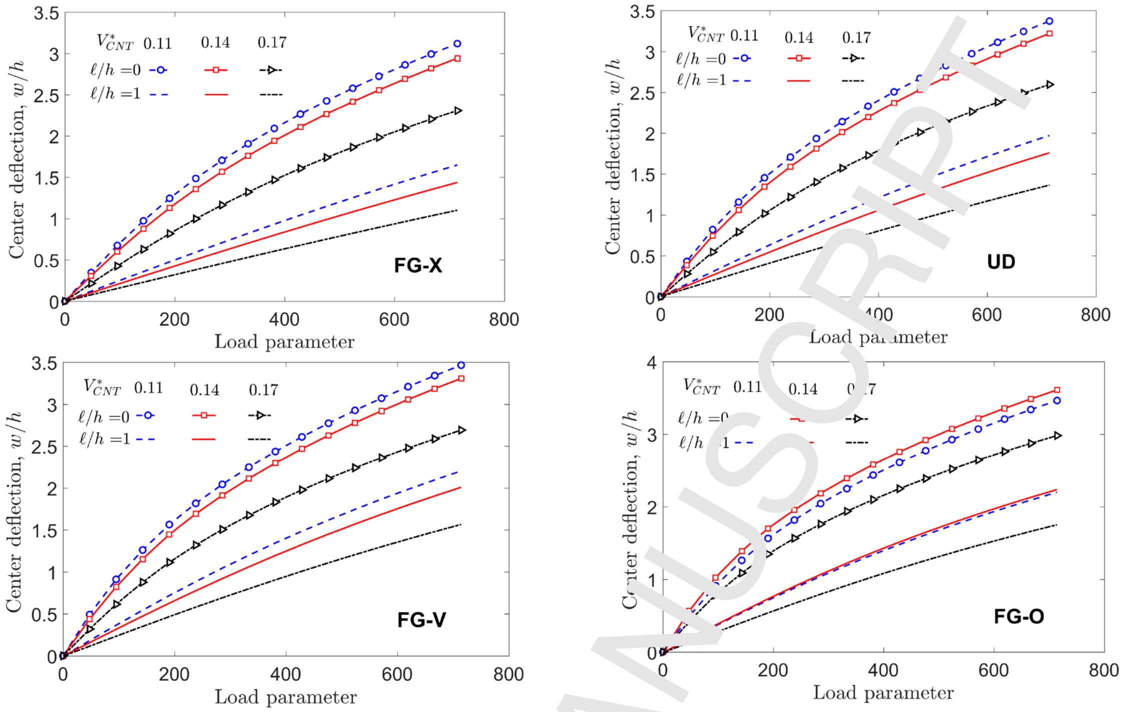

Fig. 12. The effect of volume fraction V^*_{CNT} on the load-deflection curve of FG-CNTRC micro-plate under SSSS boundary condition for the classical and MCST model.

5.2. Nonlinear dynamic analysis

In the following examples, the nonlinear dynamic behaviors of FG-CNTRC micro-plate under the transient loadings are studied in detail. In all examples, the plates are subjected to uniform transverse distributed load in any instant of time, which is $q = q_0 F(t)$, in which $F(t)$ is the load factor defined as follows:

$$F(t) = \begin{cases} \begin{cases} 1 & 0 \le t \le t_1 \\ 0 & t > t_1 \end{cases} & \text{Step load} \\ \begin{cases} 1 - t/t_1 & 0 \le t \le t_1 \\ 0 & t > t_1 \end{cases} & \text{Triangular load} \\ e^{-\lambda t} & \text{Explosive blast load} \end{cases} \tag{52}$$

where $q_0 = 10$ MPa, $\lambda = 2.5 \times 10^5\ s^{-1}$, $t_1 = 4.5 \times 10^{-9} s$ and the time history of load factor $F(t)$ is illustrated in Fig. 13.

To verify the dependency of the present model for geometrically nonlinear dynamic study, the responses of SSSS orthotropic square plate with the length L = 0.25 m and thickness h = 0.05 m under uniform step loading of $q_0 = 1$ MPa is considered with the following material properties: $E_1 = 525$ GPa, $E_2 = 21$ GPa, $G_{12} = G_{13} = G_{23} = 10.5$ GPa, and $\upsilon = 0.25$, $\rho = 800$ kg/m^3. It can be seen from Fig. 14 that the predictions of the linear and nonlinear responses show an outstanding agreement in comparison with the solutions derived from the finite strip method presented by Chen et al. [81].

Next, Figs. 15-17 illustrate the influence of small size-dependent on the nonlinear dynamic responses of FG-CNTRC micro-plate under different types of load factor. The plate's thickness is set at 17.6×10^{-6} and the length to thickness is chosen as $L/h = 20$. It is observed that as the ℓ/h increase, nonlinear displacement and periods of motion of micro-plate decrease due to the enlargement in the strength of micro-plate that come from small size effect. The MCST predictions are markedly different from the classical prediction at the ratio $\ell/h = 1$. Comparing the figures, it is seen that the triangular and explosive blast load give nearly same response, except for step load.

The effects of CNTs volume fraction on FG-X, UD, FG-V and FG-O are also described in Fig. 18. As shown, the increase in the value V_{CNT}^{*} leads to the lower magnitude of the deflection and period of motion at the level of loading owning to the more CNTs reinforced in isotropic matrix. Similarly, the nonlinear predictions of the MCTS model for four patterns of CNTs distribution are lower than those of classical model.

In the last example, the influence of structural damping on the nonlinear dynamic response of FG-CNTRC micro-plate under the step, triangular and explosive blast load is also investigated and the results are shown in Figs. 19-21. According to these figures, it can be concluded that the oscillation of the plate without damping keep continue to the end of time $t = 9\times10^{-6}$. However, by including the effect of structural damping, the geometrically nonlinear dynamic responses is reduced. The oscillation of micro-plate is extinguished after two or three cycle vibration. These behaviors can be explained that the damping has the effects of reducing and preventing the structure's oscillation. It can be concluded that the damping property of FG-CNTRC micro-plates plays an important role in the vibrational energy dissipation.

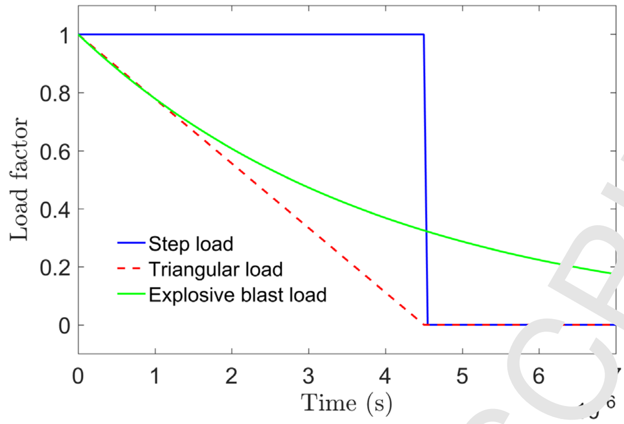

Fig. 13. Time history of load factor $F(t)$.

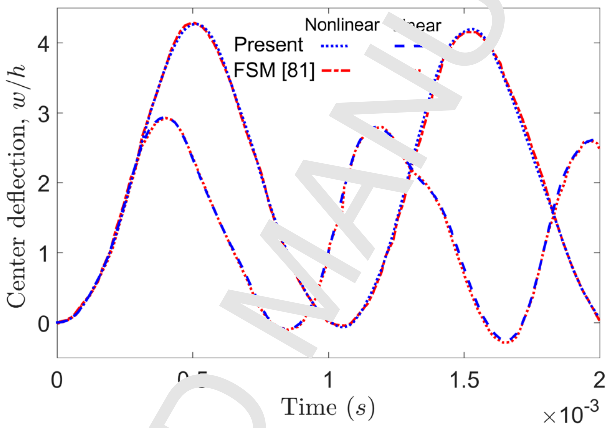

Fig. 14. Comparisons of linear and nonlinear deflections of an orthotropic plate subjected to a uniform step loading.

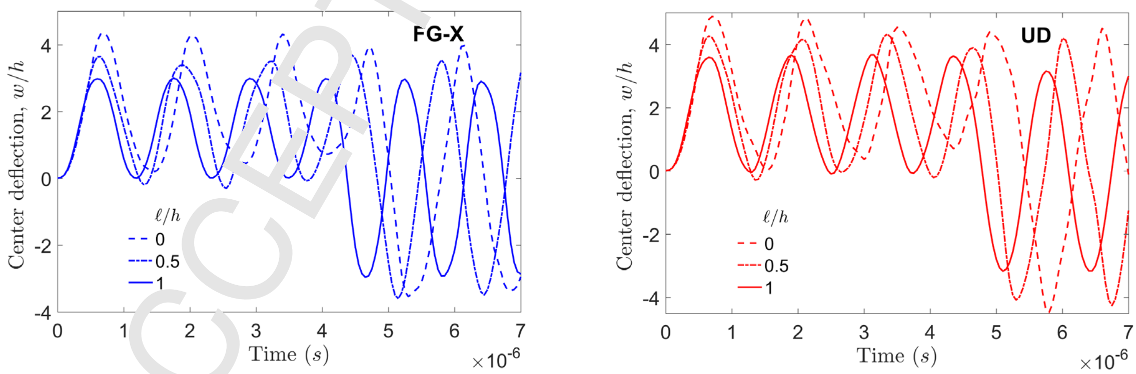

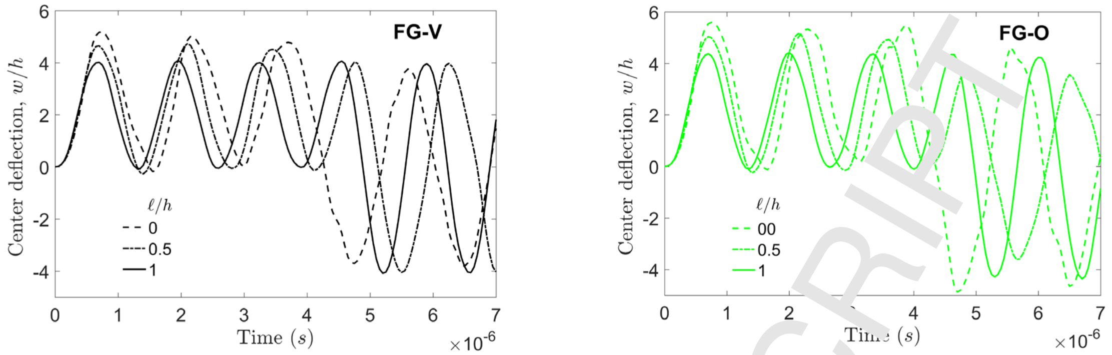

Fig. 15. The comparison of nonlinear deflections of CNT micro-plate with $V_{CNT}^{*}=0.11$ subjected to step load.

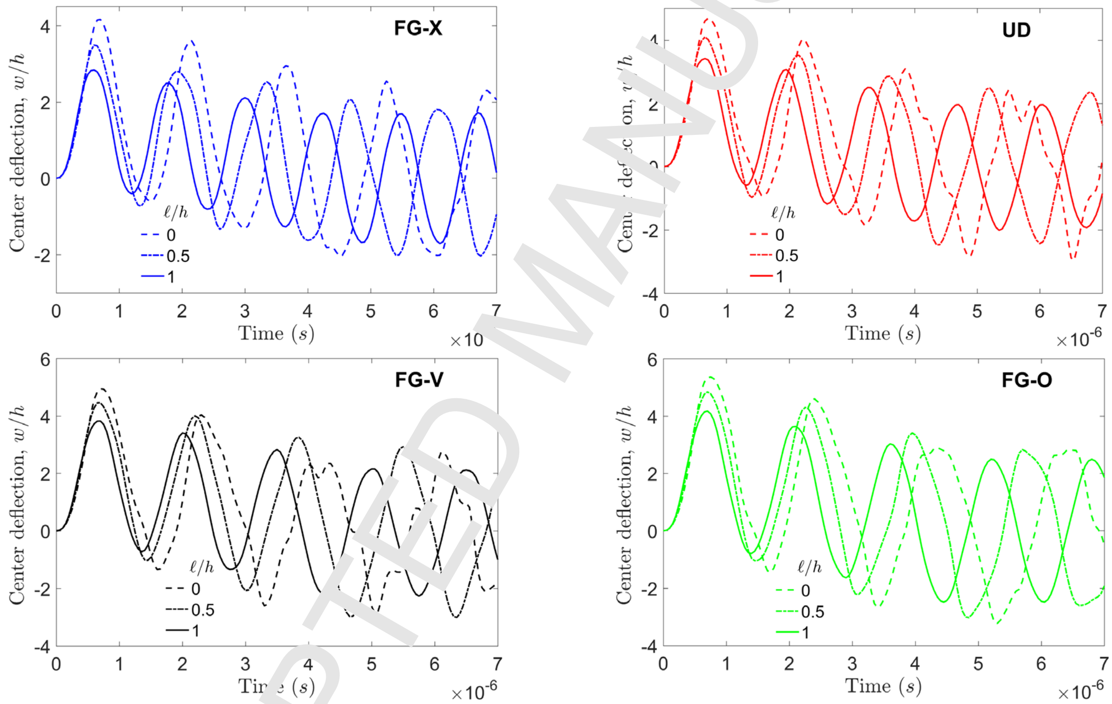

Fig. 16. The comparison of the material length scale ratios ℓ/h on nonlinear deflections of CNT micro-plate with $V_{CNT}^{*}=0.11$ subjected to triangular load.

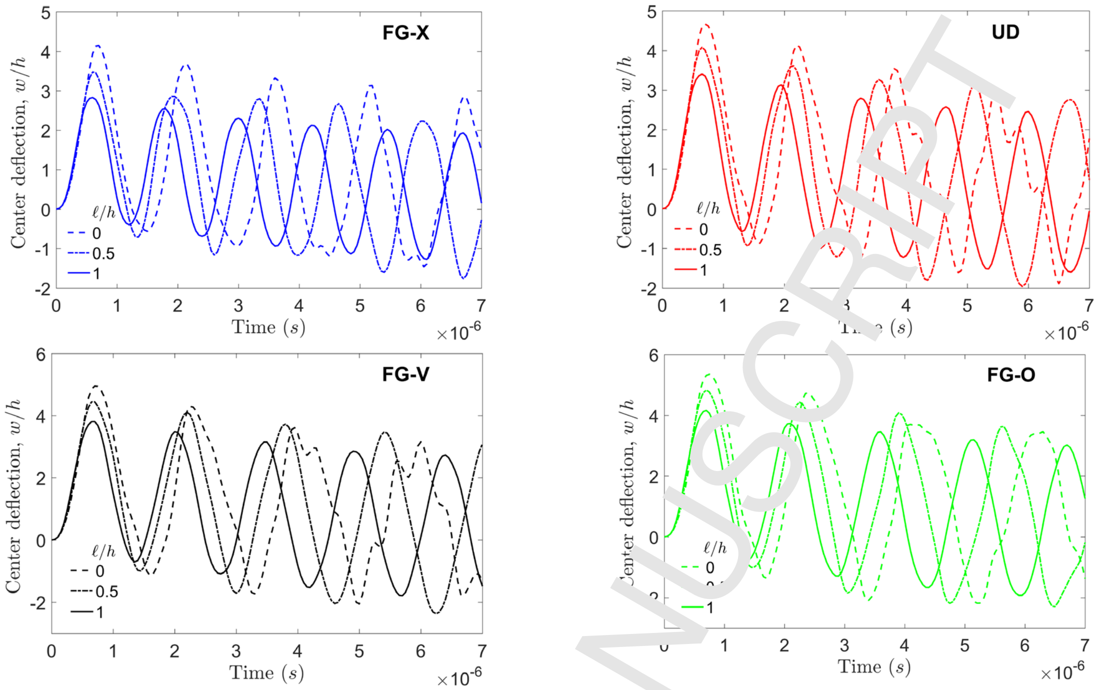

Fig. 17. The comparison of the material length scale ratios ℓ/h on nonlinear deflections of CNT micro-plate with $V^*_{CNT} = 0.11$ subjected to explosive blast load.

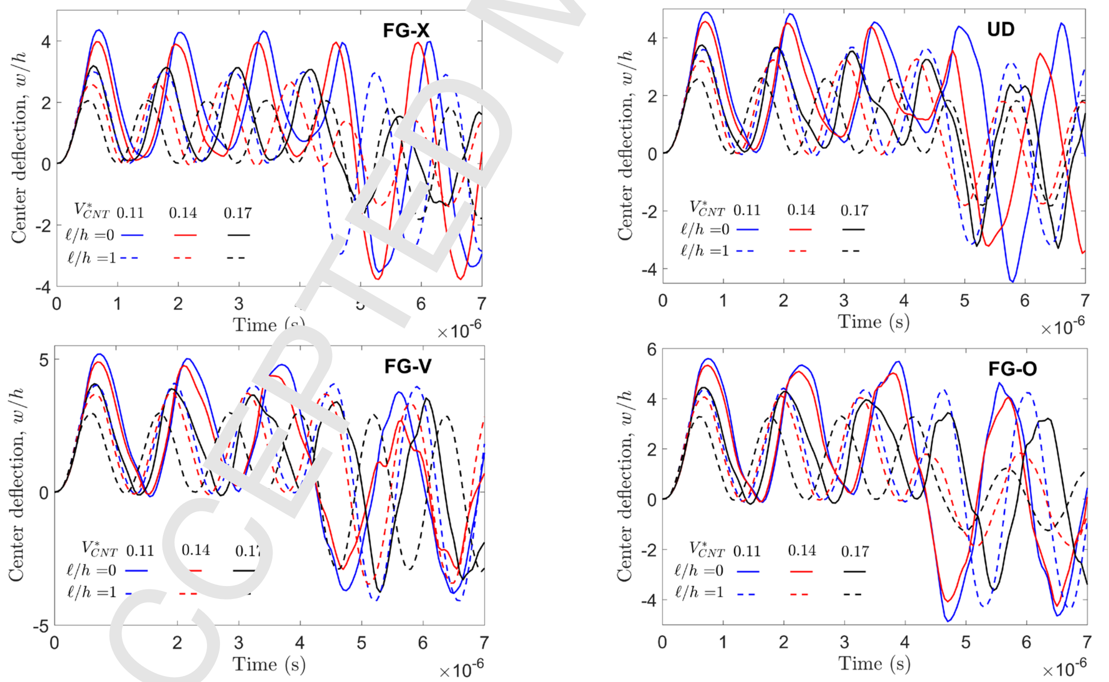

Fig. 18. The comparison of the volume fraction V^*_{CNT} on nonlinear deflections of CNT micro-plate subjected to explosive blast load for the material length scale ratios $\ell/h = 0,\ 1$.

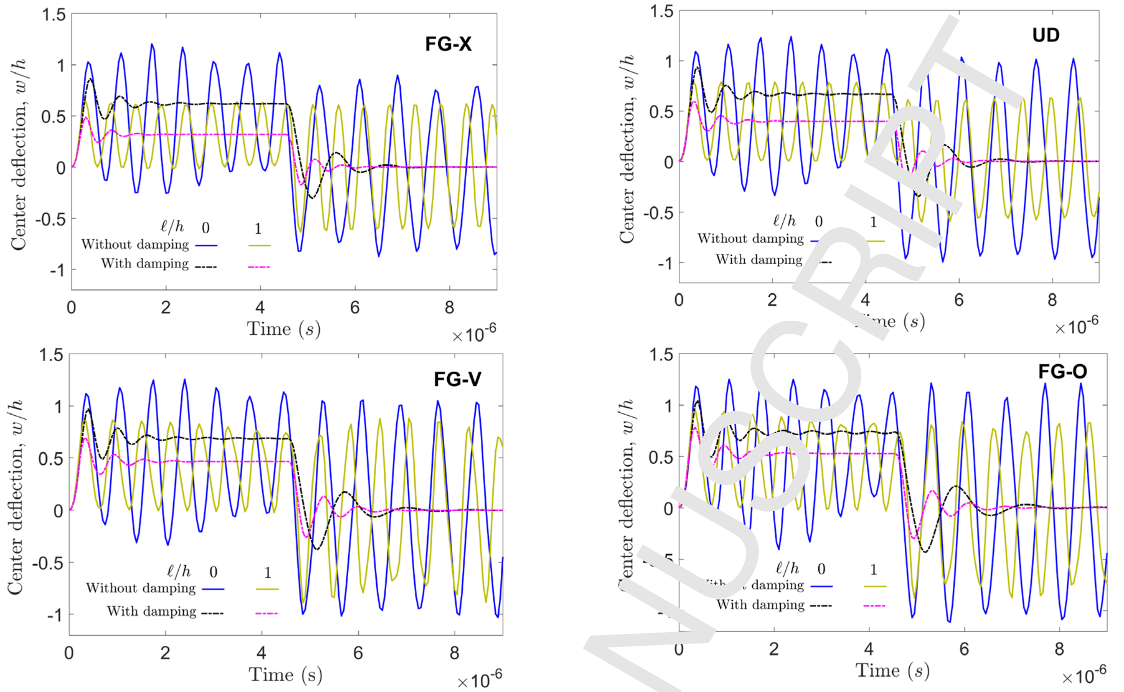

Fig. 19. Nonlinear deflections of CNT micro-plate with $V_{CNT}^{*}=0.14$ subjected to step load with and without damping.

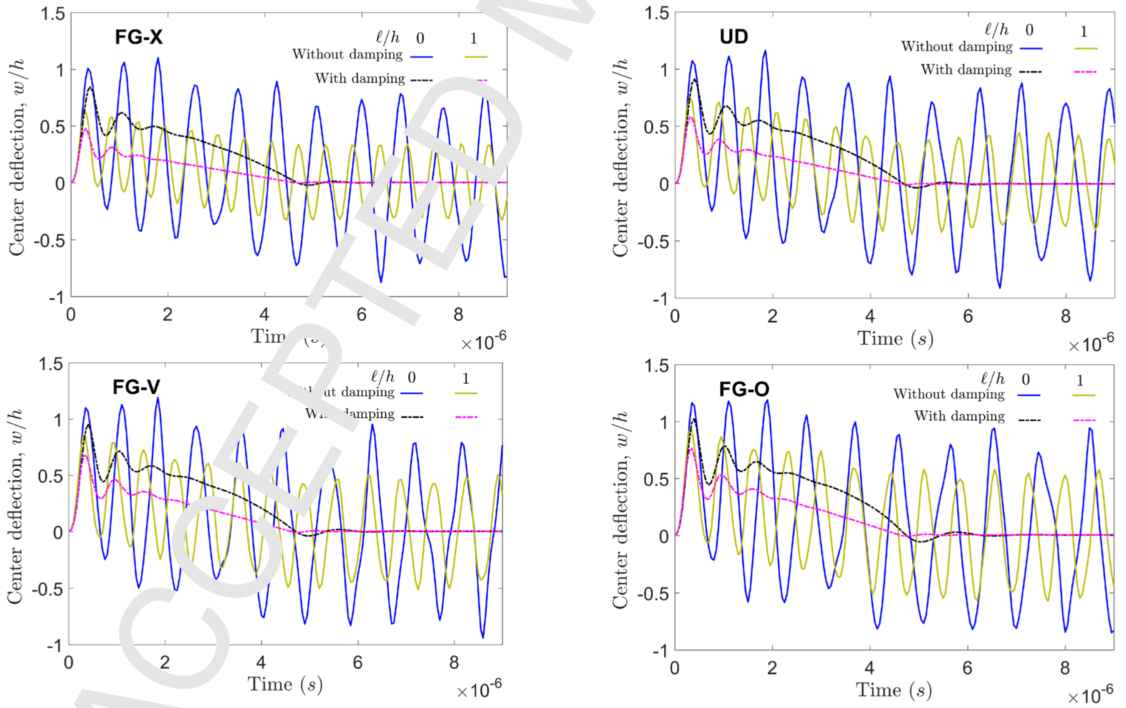

Fig. 20. Nonlinear deflections of CNT micro-plate with $V_{CNT}^{*}=0.14$ subjected to triangular load with and without damping.

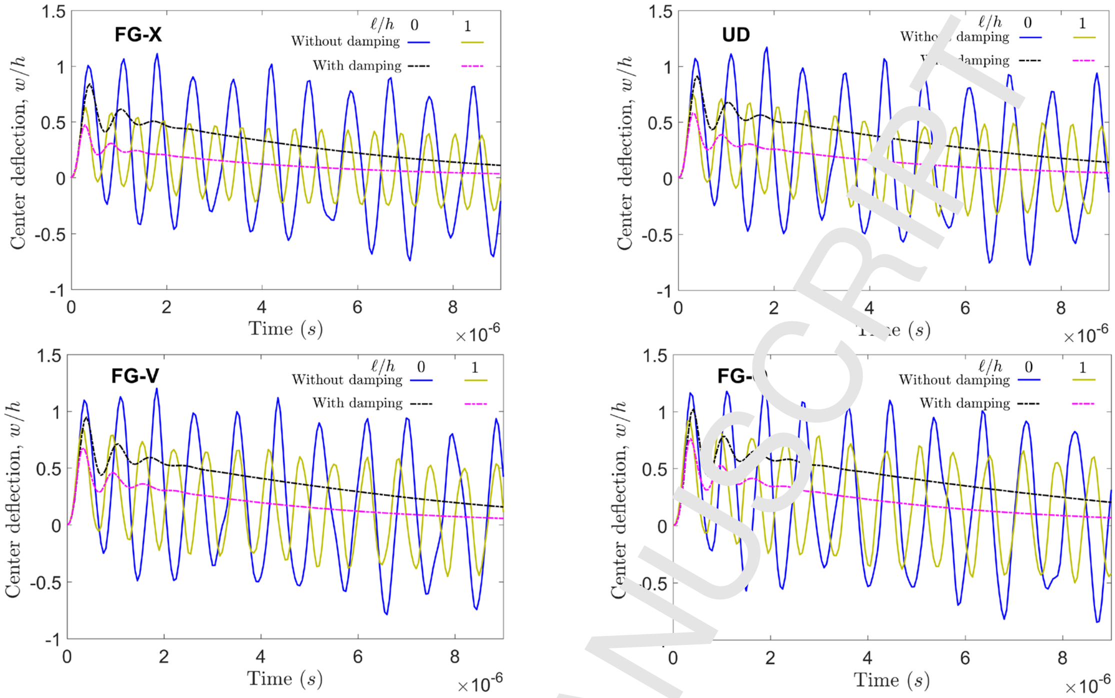

Fig. 21. Nonlinear deflections of CNT micro-plate with $V_{CNT}^{*}=0.14$ subjected to explosive blast load with and without damping.

6. Conclusions

A nonlinear numerical size-dependent model using the MCST and IGA was investigated for the nonlinear static and dynamic responses of FG-CNTRC micro-plates. The nonlinear governing equation of motion was established based on the nonlinear von-Kármán strain assumption. A proposed trigonometric shear deformation theory coupled with IGA was utilized to obtain the nonlinear displacement of plate. The proposed size-dependent using one MLS parameter can generate a classical model by set the ratio $\ell/h=0$. The faithfulness and efficacy of the proposed solution was verified through numerical examples for static and dynamic problems. The extended rule of mixture was assigned to predict the material properties of FG-CNTRC micro-plate with FG-X, UD, FG-V and FG-O carbon nanotubes distribution across the plate's thickness. Through the detailed numerical example studies, some noteworthy conclusions are summarized as follows:

- By considering only one MLS parameter, the proposed size-dependent model can easily capture the small size-dependent effect on the geometrically nonlinear responses of FG-CNTRC micro-plate. An increase in MLS ratio leads to a decrease in nonlinear static and dynamic central deflection. Thus, the MCST model produces a stiffer micro-plate compared to the classical model.

- For the patterns of CNTs distribution, at the same load level, the highest deflection is obtained for FG-O and the lowest value is obtained for FG-X.
- The increase in volume fraction V_{CNT}^{*} from 0.11 to 0.17 is denoted for the augmentation in CNTs reinforced in the isotropic matrix. Consequently, the stiffness of FG-CNTRC micro-plate tends to higher value as V_{CNT}^{*} rises.
- By including the structural damping, the nonlinear dynamic responses of FG-CNTRC micro-plate are extraordinary different from the prediction of model without damping. The damping reduces and prevents the structure's oscillation. Therefore, the damping property of CNTRC structures is important in dynamic analysis of FG-CNTRC micro-plates.

Acknowledgements

The authors acknowledge the financial support of VLIR-OUS TEAM Project, VN2017TEA454A103, 'An innovative solution to protect Vietnamese coastal riverbanks from floods and erosion', funded by the Flemish Government.

vliruos SHARING MINDS, CHANGING LIVES

With the support of THE BELGIAN DEVELOPMENT COOPERATION .be

The second author gratefully acknowledges the support of Academy of Finland (decision number 304122).

References

[1]. Li, X., B. Bhushan, K. Takashima, C.-W. Baek, and Y.-K. Kim, Mechanical characterization of micro/nanoscale structures for MEMS/NEMS applications using nanoindentation techniques. Ultramicroscopy, 2003. 97(1): p. 481-494.

[2]. Roukes, M.L., Nanoelectromechanical systems, in Transducers' 01 Eurosensors XV. 2001, Springer. p. 658-661.

[3]. Zhang, X.R. and X. Xu, Development of a biosensor based on laser-fabricatedpolymer microcantilevers. Applied physics letters, 2004. 85(12): p. 2423-2425.

[4]. McFarland, A.W. and J.S. Colton, Role of material microstructure in plate stiffness with relevance to microcantilever sensors. Journal of Micromechanics and Microengineering, 2005. 15(5): p. 1060.

[5]. Fleck, N.A., G.M. Muller, M.F. Ashby, and J.W. Hutchinson, Strain gradient plasticity: Theory and experiment. Acta Metallurgica et Materialia, 1994. 42(2): p. 475-487.

[6]. Stölken, J.S. and A.G. Evans, A microbend test method for measuring the plasticity length scale. Acta Materialia, 1998. 46(14): p. 5109-5115.

[7]. Chong, A.C.M. and D.C.C. Lam, Strain gradient plasticity effect in indentation hardness of polymers. Journal of Materials Research, 2011. 14(10): p. 4103-4110.

[8]. Lam, D.C.C., F. Yang, A.C.M. Chong, J. Wang, and P. Tong, Experiments and theory in strain gradient elasticity. Journal of the Mechanics and Physics of Solids, 2003. 51(8): p. 1477-1508.

[9]. Toupin, R.A., Elastic materials with couple-stresses. Archive for Rational Mechanics and Analysis, 1962. 11(1): p. 385-414.

[10]. Mindlin, R.D. and H.F. Tiersten, Effects of couple-stresses in linear elasticity. Archive for Rational Mechanics and Analysis, 1962. 11(1): p. 415-448.

[11]. Koiter, W.T., Couple stresses in the theory of elasticity, I and II. Nederl. Akad. Wetensch. Proc. Ser, 1964. B67: p. 17-44.

[12]. Fleck, N.A. and J.W. Hutchinson, A reformulation of strain gradient plasticity. Journal of the Mechanics and Physics of Solids, 2001. 49(10): p. 2245-2271.

[13]. Yang, F., A.C.M. Chong, D.C.C. Lam, and P. Tong, Couple stress based strain gradient theory for elasticity. International Journal of Solids and Structures, 2002. 39(10): p. 2731-2743.

[14]. Lu, P., P. Zhang, H. Lee, C. Wang, and J. Reddy. Non-local elastic plate theories. in Proceedings of the royal society of london a: Mathematical, physical and engineering sciences. 2007. The Royal Society.

[15]. Duan, W. and C.M.J.N. Wang, Exact solutions for axisymmetric bending of micro/nanoscale circular plates based on nonlocal plate theory. 2007. 18(38): p. 385704.

[16]. Reddy, J.N., Nonlocal nonlinear formulations for bending of classical and shear deformation theories of beams and plates. International Journal of Engineering Science, 2010. 48(11): p. 1507-1518.

[17]. Nguyen, N.-T., D. Hui, J. Lee, and H. Nguyen-Xuan, An efficient computational approach for size-dependent analysis of functionally graded nanoplates. Computer Methods in Applied Mechanics and Engineering, 2015. 297: p. 191-218.

[18]. Thai, H.-T., T.P. Vo, T.-K. Nguyen, and J. Lee, Size-dependent behavior of functionally graded sandwich microbeams based on the modified couple stress theory. Composite Structures, 2015. 123: p. 337-349.

[19]. Wang, Y.-G., W.-H. Lin, and N. Liu, Large amplitude free vibration of size-dependent circular micro-plates based on the modified couple stress theory. International Journal of Mechanical Sciences, 2013. 71: p. 51-57.

[20]. Wang, Y.-G., W.-H. Lin, and C.-L. Zhou, Nonlinear bending of size-dependent circular micro-plates based on the modified couple stress theory. Archive of Applied Mechanics, 2014. 84(3): p. 391-400.

[21]. Gao, X.-L., J. Huang, and J. Reddy, A non-classical third-order shear deformation plate model based on a modified couple stress theory. Acta Mechanica, 2013. 224(11): p. 2699-2718.

[22]. Reddy, J.N. and J. Kim, A nonlinear modified couple stress-based third-order theory of functionally graded plates. Composite Structures, 2012. 94(3): p. 1128-1143.

[23]. Nguyen, H.X., T.N. Nguyen, M. Abdel-Wahab, S.P.A. Bordas, H. Nguyen-Xuan, and T.P. Vo, A refined quasi-3D isogeometric analysis for functionally graded micro-plates based on the modified couple stress theory. Computer Methods in Applied Mechanics and Engineering, 2017. 313: p. 904-940.

[24]. Thanh, C.-L., L.V. Tran, T. Vu-Huu, and M. Abdel-Wahab, The size-dependent thermal bending and buckling analyses of composite laminate micro-plate based on new modified couple stress theory and isogeometric analysis. Computer Methods in Applied Mechanics and Engineering, 2019.

[25]. Karami, B., D. Shahsavari, M. Janghorban, and A. Tounsi, Resonance behavior of functionally graded polymer composite nanoplates reinforced with graphene nanoplatelets. International Journal of Mechanical Sciences, 2019. 156: p. 94-105.

[26]. Karami, B., M. Janghorban, and A. Tounsi, Variational approach for wave dispersion in anisotropic doubly-curved nanoshells based on a new nonlocal strain gradient higher order shell theory. Thin-Walled Structures, 2018. 129: p. 251-264.
[27]. Karami, B. and M. Janghorban, Characteristics of elastic waves in radial direction of anisotropic solid sphere, a new closed-form solution. European Journal of Mechanics - A/Solids, 2019. 76: p. 36-45.
[28]. Karami, B. and M. Janghorban, On the dynamics of porous nanotubes with variable material properties and variable thickness. International Journal of Engineering Science, 2019. 136: p. 53-66.
[29]. Karami, B., M. Janghorban, and A. Tounsi, Nonlocal strain gradient 3D elasticity theory for anisotropic spherical nanoparticles. Steel and composite structures, 2018. 27(2): p. 201-216.
[30]. Ansari, R., R. Gholami, M. Faghih Shojaei, V. Mohammadi, and M.A. Darabi, Thermal Buckling Analysis of a Mindlin Rectangular FGM Micro-plate Based on the Strain Gradient Theory. Journal of Thermal Stresses, 2013. 36(5): p. 446-465.
[31]. Torabi, J., R. Ansari, and M. Darvizeh, Application of a non-conforming tetrahedral element in the context of the three-dimensional strain gradient elasticity. Computer Methods in Applied Mechanics and Engineering, 2019. 344: p. 1124-1143.
[32]. Sahmani, S. and R.J.C.S. Ansari, On the free vibration response of functionally graded higher-order shear deformable micro-plates based on the strain gradient elasticity theory. 2013. 95: p. 430-442.
[33]. Karami, B., D. Shahsavari, M. Janghorban, and L. Li, Influence of homogenization schemes on vibration of functionally graded curved microbeams. Composite Structures, 2019. 216: p. 67-79.
[34]. Thostenson, E.T., Z. Ren, T.-W. Chou, and technology, Advances in the science and technology of carbon nanotubes and their composites: a review. Composites science technology, 2001. 61(13): p. 1899-1912.
[35]. Wan, H., F. Delale, and L. Shen, Effect of CNT length and CNT-matrix interphase in carbon nanotube (CNT) reinforced composites. Mechanics Research Communications, 2005. 32(5): p. 481-489.
[36]. Spitalsky, Z., D. Tasis, K. Papagelis, and C. Galiotis, Carbon nanotube–polymer composites: Chemistry, processing, mechanical and electrical properties. Progress in Polymer Science, 2010. 35(3): p. 357-401.
[37]. Kwon, H., C.R. Bradbury, and M. Leparoux, Fabrication of Functionally Graded Carbon Nanotube-Reinforced Aluminum Matrix Composite. Advanced engineering materials, 2011. 13(4): p. 325-329.
[38]. Khan, W., R. Sharma, and P. Saini, Carbon nanotube-based polymer composites: synthesis, properties and applications, in Carbon Nanotubes-Current Progress of their Polymer Composites. 2016, Intech Open.
[39]. Maziar Janghorban, D.S., in An Introduction to Nanostructures (Introduction, Synthesis, Applications and Modeling). 2018, NAGHOOS Publication
[40]. Ravari, M.K. and H. Zeighampour, Vibration analysis of functionally graded carbon nanotube-reinforced composite nanoplates using Mindlin's strain gradient theory. Composite Structures, 2015. 134: p. 1036-1043.
[41]. Ghorbanpour Arani, A., B. Rousta Navi, and M. Mohammadimehr, Surface stress and agglomeration effects on nonlocal biaxial buckling polymeric nanocomposite plate reinforced by CNT using various approaches. Advanced Composite Materials, 2016. 25(5): p. 423-441.
[42]. Mohammadimehr, M., B. Rousta Navi, and A. Ghorbanpour Arani, Modified strain gradient Reddy rectangular plate model for biaxial buckling and bending analysis of double-coupled piezoelectric polymeric nanocomposite reinforced by FG-SWNT. Composites Part B: Engineering, 2016. 87: p. 132-148.
[43]. Mohammadimehr, M., M. Mohandes, and M. Moradi, Size dependent effect on the buckling and vibration analysis of double-bonded nanocomposite piezoelectric plate reinforced by boron nitride

nanotube based on modified couple stress theory. Journal of Vibration and Control, 2014. 22(7): p. 1790-1807.
[44]. Karami, B., D. Shahsavari, and M. Janghorban, A comprehensive analytical study on functionally graded carbon nanotube-reinforced composite plates. Aerospace Science and Technology, 2018. 82-83: p. 499-512.
[45]. Hughes, T.J.R., J.A. Cottrell, and Y. Bazilevs, Isogeometric analysis: CAD, finite elements, NURBS, exact geometry and mesh refinement. Computer Methods in Applied Mechanics and Engineering, 2005. 194(39): p. 4135-4195.
[46]. Hughes Thomas JR, C.J.A., Bazilevs Yuri, Isogeometric analysis: CAD, finite elements, NURBS, exact geometry and mesh refinement. Computer methods in applied mechanics and engineering, 2005. 194(39): p. 4135-4195.
[47]. Tran, L.V., A. Ferreira, and H. Nguyen-Xuan, Isogeometric analysis of functionally graded plates using higher-order shear deformation theory. Composites Part B: Engineering, 2013. 51: p. 368-383.
[48]. Nguyen-Xuan, H., L.V. Tran, C.H. Thai, S. Kulasegaram, and S.P.A. Bordas, Isogeometric analysis of functionally graded plates using a refined plate theory. Composites Part B: Engineering, 2014. 64(Supplement C): p. 222-234.
[49]. Bui, T.Q., S. Hirose, C. Zhang, T. Rabczuk, C.-T. Wu, T. Saitoh, and J. Lei, Extended isogeometric analysis for dynamic fracture in multiphase piezoelectric/piezomagnetic composites. Mechanics of Materials, 2016. 97: p. 135-163.
[50]. Yin, S., T. Yu, T.Q. Bui, X. Zheng, and S. Tanaka, In-plane material inhomogeneity of functionally graded plates: A higher-order shear deformation plate isogeometric analysis. Composites Part B: Engineering, 2016. 106: p. 273-284.
[51]. Gu, J., T. Yu, L. Van Lich, T.-T. Nguyen, and T.Q. Bui, Adaptive multi-patch isogeometric analysis based on locally refined B-splines. Computer Methods in Applied Mechanics and Engineering, 2018. 339: p. 704-738.
[52]. Gu, J., T. Yu, L. Van Lich, T.-T. Nguyen, S. Tanaka, and T.Q. Bui, Multi-inclusions modeling by adaptive XIGA based on LR B-splines and multiple level sets. Finite Elements in Analysis Design, 2018. 148: p. 48-66.
[53]. Tran, L.V., J. Lee, H. Nguyen-Van, H. Nguyen-Xuan, and M.A. Wahab, Geometrically nonlinear isogeometric analysis of laminated composite plates based on higher-order shear deformation theory. International Journal of Non-Linear Mechanics, 2015. 72: p. 42-52.
[54]. Thanh, C.-L., P. Phung-Van, C.H. Thai, H. Nguyen-Xuan, and M. Abdel Wahab, Isogeometric analysis of functionally graded carbon nanotube reinforced composite nanoplates using modified couple stress theory. Composite Structures, 2018. 184(Supplement C): p. 633-649.
[55]. Thanh, C.-L., L.V. Tran, T.Q. Bui, H.X. Nguyen, and M. Abdel-Wahab, Isogeometric analysis for size-dependent nonlinear thermal stability of porous FG micro-plates. Composite Structures, 2019.
[56]. Phung-Van, P., C.-L. Thanh, H. Nguyen-Xuan, and M. Abdel-Wahab, Nonlinear transient isogeometric analysis of FG-CNTRC nanoplates in thermal environments. Composite Structures, 2018. 201: p. 882-892.
[57]. Liu, S., T. Yu, and T.Q. Bui, Size effects of functionally graded moderately thick micro-plates: A novel non-classical simple-FSDT isogeometric analysis. European Journal of Mechanics - A/Solids, 2017. 66: p. 446-458.
[58]. Phung-Van, P., Q.X. Lieu, H. Nguyen-Xuan, and M.A. Wahab, Size-dependent isogeometric analysis of functionally graded carbon nanotube-reinforced composite nanoplates. Composite Structures, 2017. 166: p. 120-135.
[59]. Phung-Van, P., C.H. Thai, H. Nguyen-Xuan, and M. Abdel Wahab, Porosity-dependent nonlinear transient responses of functionally graded nanoplates using isogeometric analysis. Composites Part B: Engineering, 2019. 164: p. 215-225.

[60]. Liu, S., T. Yu, L.V. Lich, S. Yin, and T.Q. Bui, Size and surface effects on mechanical behavior of thin nanoplates incorporating microstructures using isogeometric analysis. Computers & Structures, 2019. 212: p. 173-187.

[61]. Gou, J., S. O'Braint, H. Gu, and G. Song, Damping augmentation of nanocomposites using carbon nanofiber paper. Journal of nanomaterials, 2006.

[62]. Lass, E., N. Koratkar, P. Ajayan, B. Wei, and P. Keblinski, Damping and stiffness enhancement in composite systems with carbon nanotubes films. MRS Online Proceedings Library Archive, 2002. 740.

[63]. Kordani, N., A. Fereidoon, and M. Ashoori, Damping augmentation of nanocomposites using carbon nanotube/epoxy. Structural Dynamics, 2011. 3: p. 1605-1615.

[64]. Shi D-L, F.X.-Q., Huang YY, Hwang K-C, Gao H, The effect of nanotube waviness and agglomeration on the elastic property of carbon nanotube reinforced composites. J Eng Mater Technol, 2004. 126: p. 250-7.

[65]. Zhu P, L.Z., Liew KM, Static and free vibration analyses of carbon nano-tube reinforced composite plates using finite element method with first order shear deformation plate theory Compos Struct, 2012. 94: p. 1450-60.

[66]. Esawi, A.M., M.M. Farag, and design, Carbon nanotube reinforced composites: potential and current challenges. Materials design, 2007. 28(9): p. 2394-2401.

[67]. Shen, H.-S., Nonlinear bending of functionally graded carbon nanotube-reinforced composite plates in thermal environments. Composite Structures, 2009. 91(1): p. 9-19.

[68]. Zhang, C.-L. and H.-S. Shen, Temperature-dependent elastic properties of single-walled carbon nanotubes: prediction from molecular dynamics simulation. Applied Physics Letters, 2006. 89(8): p. 081904.

[69]. Zenkour, A.M., Buckling of fiber-reinforced viscoelastic composite plates using various plate theories. Journal of Engineering Mathematics, 2004. 50(1): p. 75-93.

[70]. Zenkour, A.M., Generalized shear deformation theory for bending analysis of functionally graded plates. Applied Mathematical Modelling, 2006. 30(1): p. 67-84.

[71]. Thai, C.H., S. Kulasegaram, L.V. Tran, and H. Nguyen-Xuan, Generalized shear deformation theory for functionally graded isotropic and sandwich plates based on isogeometric approach. Computers & Structures, 2014. 141: p. 94-112.

[72]. Reddy, J.N., A simple higher-order theory for laminated composite plates. Journal of applied mechanics, 1984. 51(4): p. 745-752.

[73]. Soldatos, K., A transverse shear deformation theory for homogeneous monoclinic plates. Acta Mechanica, 1992. 94(3-4): p. 195-220.

[74]. Nguyen-Xuan, H., C.H. Thai, and T. Nguyen-Thoi, Isogeometric finite element analysis of composite sandwich plates using a higher order shear deformation theory. Composites Part B: Engineering, 2013. 55: p. 558-574.

[75]. Thai, C.H., A.J.M. Ferreira, T. Rabczuk, and H. Nguyen-Xuan, Size-dependent analysis of FG-CNTRC micro-plates based on modified strain gradient elasticity theory. European Journal of Mechanics - A/Solids, 2018. 72: p. 521-538.

[76]. Liu, S., T. Yu, T.Q. Bui, and S. Xia, Size-dependent analysis of homogeneous and functionally graded micro-plates using IGA and a non-classical Kirchhoff plate theory. Composite Structures, 2017. 172: p. 34-44.

[77]. Clough, R.W. and J. Penzien, Dynamics of Structures. Berkeley: Computers & Structures. 1995, Inc.

[78]. Popov, V., V. Van Doren, and M. Balkanski, Elastic properties of crystals of single-walled carbon nanotubes. Solid State Communications, 2000. 114(7): p. 395-399.

[79]. Zhang, L.W., Z.G. Song, and K.M. Liew, Nonlinear bending analysis of FG-CNT reinforced composite thick plates resting on Pasternak foundations using the element-free IMLS-Ritz method. Composite Structures, 2015. 128: p. 165-175.

[80]. Kim, J. and J.N. Reddy, A general third-order theory of functionally graded plates with modified couple stress effect and the von Kármán nonlinearity: theory and finite element analysis. Acta Mechanica, 2015. 226(9): p. 2973-2998.

[81]. Chen, J., D.J. Dawe, and S. Wang, Nonlinear transient analysis of rectangular composite laminated plates. Composite Structures, 2000. 49(2): p. 129-139.

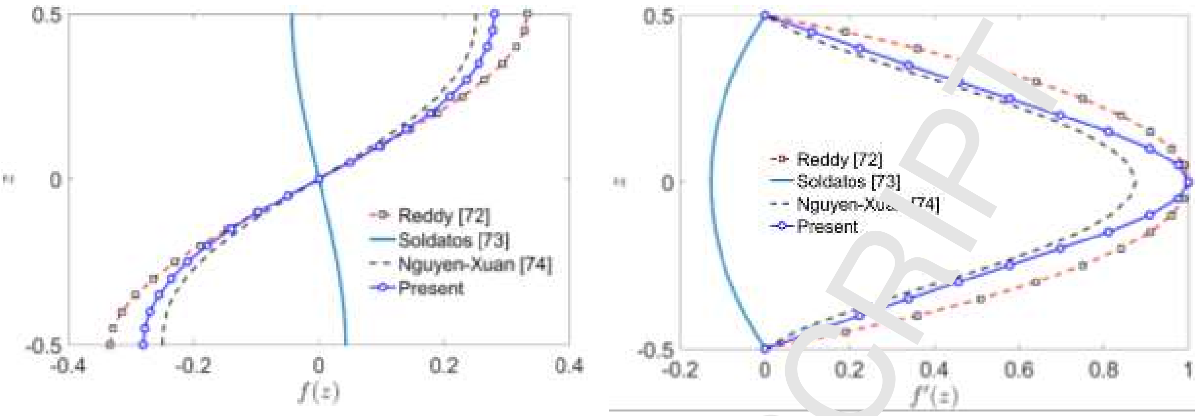

Fig. 1. Shape function $f(z)$ and its first derivative $f'(z)$ across the plate's thickness.

Highlights

- A nonlinear numerical model functionally graded carbon nanotube reinforced composite (FG-CNTRC) micro-plate
- Modified couple stress theory (MCST) coupled with trigonometric shear deformation theory coupled with isogeometric analysis
- Influence of damping characteristic on the oscillation of FG-CNTRC micro-plates